Linear waves at viscoelastic interfaces between viscoelastic media

Sina Zendehroud [1], Roland R. Netz [1,*] and Julian Kappler [1,2]

[1]*Freie Universität Berlin, Department of Physics, Arnimallee 14, 14195 Berlin, Germany*
[2]*University of Cambridge, Wilberforce Road, DAMTP, Centre for Mathematical Sciences,
Cambridge CB3 0WA, United Kingdom*

We derive the general dispersion relation for interfacial waves along a planar viscoelastic boundary that separates two viscoelastic bulk media, including the effect of gravity. Our unified theory contains Rayleigh waves, capillary-gravity-flexural waves, Lucassen waves, bending waves in elastic plates, and the standard dispersion-free sound waves, as limiting cases. To illustrate our results, we consider waves at a viscoelastic interface immersed in water and at an air-water interface. We furthermore investigate waves at a viscoelastic interface separating two identical viscoelastic bulk media, for which we consider both Kelvin-Voigt and Maxwell materials, as applicable to polymer gels and solutions. For all cases, we study how material properties determine the crossovers, scaling, and existence regimes of the various interfacial waves. Since we include viscoelastic effects for all media involved, our theory allows to model waveguiding phenomena in biology, such as pressure pulses in axon membranes, which are possibly relevant for acoustic nerve pulse propagation phenomena.

I. INTRODUCTION

Waves at interfaces are well known and can be observed in everyday life. A classical example is the capillary-gravity wave on an incompressible Newtonian fluid under the influence of gravity [1–6]. For high enough frequencies, the capillarity dominates over the effects of gravity and the dynamics of the capillary wave is dominated by the effects of surface tension; the displacement of the interface is then predominantly perpendicular to the interface. The theory of this wave has been extended to include interfacial properties, such as bending rigidity [7], and to include viscoelastic shear response in the bulk, as applicable to, e.g., gels [8]. If the interface responds viscoelastically to compression, then a second type of surface wave can coexist with the capillary-gravity wave. We refer to this interfacial pressure wave as Lucassen wave [9–12]; it has recently received attention because of its possible relevance for acoustic nerve pulse propagation [13–16]. The Lucassen wave is essentially a sound wave along the interface and its displacement is predominantly in the plane of the interface. For elastic materials where the interfacial properties are negligible, a third kind of surface wave exists, which is called the Rayleigh wave [17]. While for a purely elastic material only one such solution exists, for a viscoelastic material, two wave solutions with distinct dispersion relations can coexist [18,19]. Viscoelastic Rayleigh waves are of particular interest, e.g., in geophysics, as a model for earthquake-generated waves [20], or in material engineering, to noninvasively measure mechanical properties of media [21]. In a scenario where gravitation, surface tension and bulk shear viscosity are simultaneously nonzero, capillary-gravity-viscous (CGV) surface waves can exist, which are different from all the above waves, and have only very recently been discovered [22].

---

*Corresponding author: rnetz@physik.fu-berlin.de

Localized waves at fluid interfaces have recently gained renewed attention in the search of a more complete picture of nerve pulse propagation [23–29]. While the standard Hodgkin-Huxley model is successful in modeling the observed electrical phenomena, it is known that a mechanical displacement propagates alongside the electrical pulse [30,31]. The biological relevance of these mechanical waves is not resolved conclusively, however, it has been conjectured that mechanical waves accompanying the action potential serve a physiological function and that inclusion of these mechanical phenomena into existing theories would provide a more complete picture of nerve pulse propagation [23–29].

For the modeling of biologically relevant surface wave phenomena, a natural theoretical model is given by a viscoelastic interface separating two viscoelastic media. In the biological setting, e.g., when comparing the axoplasm to the extracellular fluid separated by an axon membrane, the bulk media on both sides will rarely differ so much as to justify neglecting one of them. Hydrodynamic modes of a thin viscoelastic material at the interface between two Newtonian fluids were already discussed in Ref. [32]. The dynamics of viscoelastic membranes separating two Newtonian fluids have been studied with regard to microrheological studies of such membranes [33]. Recently, a comprehensive dispersion relation has been derived for linear waves at a surfactant layer separating two Newtonian fluids, supporting capillary-gravity waves and Lucassen waves as solutions [34,35]. However, the general case of two in general different viscoelastic media separated by a viscoelastic interface has not been considered before.

For a single viscoelastic half-space, which is an appropriate model if one of the bulk media is negligible, recently a general surface wave dispersion relation was derived, which contains Rayleigh, capillary-gravity, and Lucassen waves as limiting cases [22]. This allowed to discuss the relation between those waves: For water, modeled as an almost incompressible viscoelastic medium, the Lucassen wave transforms into a Rayleigh wave at high frequencies. Waves on half-spaces of a viscoelastic solid were investigated numerically in order to model rheological applications in Refs. [36,37], while capillary waves on viscoelastic half-spaces have been studied numerically in Refs. [38,39].

If the media at the two sides of an elastic interface can be neglected, then transversal oscillations of the interface are described by elastic plate theory [40], while compression waves within the interface are described by a standard wave equation.

For capillary-gravity waves, the relation between the model of two fluid half-spaces and the model of just one fluid half-space has been explored [34], but the general relation between the theories for interfacial waves with two fluid half-spaces, one fluid half-space, and an oscillating plate in vacuum, has not been discussed.

In the present work, we derive the general dispersion relation for waves at planar viscoelastic interfaces separating two different linear isotropic homogeneous viscoelastic half-spaces including the effects of gravity. By considering a general dispersion relation, we quantify the existence regimes of each of the aforementioned wave solutions and assess which material properties are relevant for the respective wave modes and frequency regimes. We show how the interfacial capillary-gravity and Lucassen waves follow from a factorization of the general dispersion relation. After considering the symmetric case, where the two bulk media have the same properties, we then first discuss the limit where one of the bulk media is negligible, and second the limit where both bulk media can be neglected. Our theory furthermore allows us to study the interrelations of the various limiting cases. For example, our derivation shows explicitly that the elastic plate equation can be considered as a limit of the capillary-gravity-flexural wave, i.e., the capillary-gravity wave for an interface with bending rigidity, a result which we have not encountered in the existing literature. The one-dimensional wave equation, in turn, is recovered as a limit of the Lucassen wave.

We go on to discuss several explicit scenarios. We consider localized waves at a water-water interface, and at an air-water interface (where we show that the half-space of air can be neglected). We then consider the case of an interface separating two viscoelastic bulk media, modeled via Kelvin-Voigt and Maxwell materials, respectively. For every explicit scenario, we highlight the
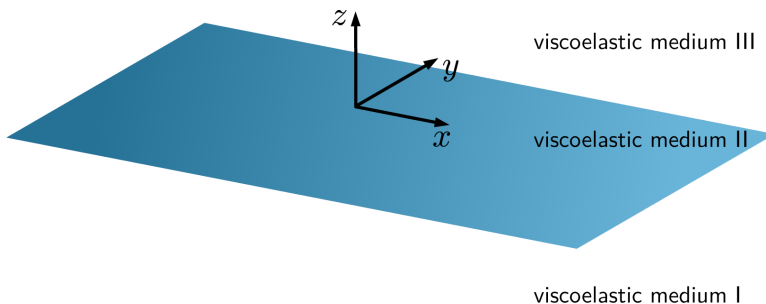
FIG. 1. We consider a planar viscoelastic interface (medium II), which is located at $z = 0$ and separates two viscoelastic bulk media (media I and III), which are infinitely extended in the half-spaces $z < 0$, $z > 0$. All viscoelastic media are modeled as linear, isotropic, and homogeneous. We include gravitational acceleration, which acts in the negative z direction. We consider wave solutions that travel in the x direction, and are translationally invariant in y, and decay exponentially away from the interface at $z = 0$.

different power-law scalings of phase velocities and propagation distances emerging from the model.

The organization of this paper is as follows: In Sec. II we establish the framework of our calculations and derive a general dispersion relation for our setup: In Sec. II A we review linear viscoelasticity and explain how the viscoelastic properties of the interface enter the theory in the form of boundary conditions. In Sec. II B we demonstrate how, for our setup, the harmonic wave ansatz leads to a conditional equation whose solutions describe traveling waves localized at the interface. In Sec. II C we show that the conditional equation factorizes under appropriate conditions, leading to generalized approximate dispersion relations for capillary-gravity-flexural waves and Lucassen waves. In Sec. III we discuss how special cases known from the literature arise in various limits, namely, the symmetric case, where media I and III are equal, the situation where medium III is absent, here called asymmetric case, and waves on a free membrane. In Sec. IV, after a review of viscoelastic relaxation functions for Newtonian fluids, we then consider numerical solutions of both the general dispersion relation and the appropriate limits, focusing on waves at the water-water interface and on waves at the air-water interface, showing that air is mostly negligible when paired with water. We investigate interfaces of viscoelastic bulk media, specifically polymer gels, modeled as Kelvin-Voigt materials, and concentrated polymer solutions, modeled as Maxwell-fluids. For all example systems, we discuss the different power-law scalings and crossovers in detail. Finally, in Sec. V we summarize our findings and discuss implications as well as applications.

Because there is a great variety of notations in hydrodynamics and viscoelasticity theory, we have compiled a list of all material parameters appearing in this paper in Appendix A.

II. GENERAL DISPERSION RELATION FOR WAVES AT VISCOELASTIC INTERFACES

We study localized waves at a viscoelastic interface between two viscoelastic media, as illustrated in Fig. 1. We choose the coordinate system such that the interface is at $z = 0$, and refer to the bulk media in the lower and upper half-spaces as medium I and medium III, respectively. The interface itself we call medium II. We assume all displacements to be small, and use the linear theory of viscoelasticity for the description of media I and III. Medium II enters the dynamics via the boundary conditions at the interface.

The following derivation is a generalization of Ref. [22] and follows the standard derivation of Rayleigh waves [17].

A. Linear viscoelasticity

In each of the two bulk media, the linearized equations for momentum conservation are given at a position $\boldsymbol{r} = (x, y, z)$ and time t as [41]

$$\rho_M(\boldsymbol{r}, t)\partial_t^2 u_{M,j}(\boldsymbol{r}, t) = \partial_k \sigma_{M,jk}(\boldsymbol{r}, t) + F_{M,j}(\boldsymbol{r}, t) \tag{1}$$

for $j \in \{x, y, z\}$, where $M \in \{\text{I, III}\}$ denotes the bulk medium, so that for $z < 0$ we have $M = \text{I}$ and for $z > 0$ we have $M = \text{III}$, $\rho_M(\boldsymbol{r}, t)$ is the respective mass density, $\boldsymbol{u}_M(\boldsymbol{r}, t)$ is the displacement field, $\boldsymbol{F}_M(\boldsymbol{r}, t)$ is an external force, and where we use the Einstein summation convention for repeated indices. We assume linear, isotropic, and homogeneous bulk media, for which the stress tensor components $\sigma_{M,jk}(\boldsymbol{r}, t)$ depend on the displacement via the viscoelastic stress-strain relation [41]

$$\sigma_{M,jk}(\boldsymbol{r}, t) = \int_{-\infty}^{\infty} g_{M,\text{s}}(t - t')\partial_{t'}\epsilon_{M,jk}(\boldsymbol{r}, t')\, dt'$$
$$+ \frac{\delta_{jk}}{3}\int_{-\infty}^{\infty}[g_{M,\text{d}}(t - t') - g_{M,\text{s}}(t - t')]\partial_{t'}\epsilon_{M,ll}(\boldsymbol{r}, t')\, dt', \tag{2}$$

where the components of the strain tensor are given by $\epsilon_{M,jk} = (\partial_j u_{M,k} + \partial_k u_{M,j})/2$, and by the Einstein summation convention we have $\epsilon_{M,ll} = \partial_l u_{M,l} = \nabla \cdot \boldsymbol{u}_M$. For homogeneous media, the shear and dilational relaxation functions $g_{M,\text{s}}(t)$, $g_{M,\text{d}}(t)$ are independent of position, and to ensure causality are equal to zero for negative arguments t. With our parametrization (2) we can model any linear, isotropic, and homogenous compressible bulk medium. In Sec. IV we consider three different models for the bulk fluids, namely, the Newtonian, Kelvin-Voigt, and Maxwell fluid models. In these cases, the response functions $g_{M,\text{s}}$ and $g_{M,\text{d}}$ can be written in terms of viscosities and elastic moduli. We note that while water is usually modeled as a Newtonian fluid, in the THz regime the Newtonian fluid model needs to be replaced by more general relaxation functions [42]. For the interface, medium II, we assume a purely viscous shear response with viscosity $\eta_{2\text{D}}$, a viscoelastic response under dilation with viscosity $\eta'_{2\text{D}}$, and a position-dependent surface tension $\sigma_{2\text{D}}(\boldsymbol{r}, t)$, as explained in Appendix C. For out of plane deformations, we consider a bending rigidity $\kappa_{2\text{D}}$ and a transverse viscosity $\eta_{2\text{D}}^{\perp}$, which accounts for the lateral friction between molecules in the interfacial zone [43]. Furthermore, the interface has a surface excess mass area density $\rho_{2\text{D}}$. The surface excess mass is defined as the difference of the actual mass present close to the interface of the system and the mass of a reference system in which the bulk concentrations in the two phases remain uniform up to the interface [44]. A review for the derivation of the continuum-mechanical boundary conditions of two bulk media divided by such a viscoelastic interface was given by Kralchevsky *et al.* [43]; the resulting linearized stress-continuity condition for the displacement field at $z = 0$ has been derived in Ref. [22] and is reproduced in Appendix C. Further below, we use this continuity condition to relate the two solutions $\boldsymbol{u}_\text{I}(\boldsymbol{r}, t)$, $\boldsymbol{u}_\text{III}(\boldsymbol{r}, t)$ at the interface $z = 0$.

We consider gravity as external force, $\boldsymbol{F}_M(\boldsymbol{r}, t) = -g\rho_M\hat{\boldsymbol{e}}_z$, where $g = 9.81\ \text{m/s}^2$ is the gravitational acceleration and $\hat{\boldsymbol{e}}_z$ is the unit vector pointing in the positive z direction. We use the surface gravity approximation [45], for which the effect of gravity on media I, II, and III, enters only at the boundary condition $z = 0$ and not in the equations of motion of the bulk media; for more details see Ref. [22].

B. Harmonic wave ansatz and resulting dispersion relation

To solve the momentum conservation Eq. (1) for bulk medium M, we describe the displacement fields $\boldsymbol{u}_M(\boldsymbol{r}, t)$ via displacement potentials $\varphi_M(\boldsymbol{r}, t)$, $\boldsymbol{\psi}_M(\boldsymbol{r}, t)$ as

$$\boldsymbol{u}_M = \nabla\varphi_M + \nabla \times \boldsymbol{\psi}_M. \tag{3}$$

If the temporal Fourier transforms of the displacement potentials satisfy the Helmholtz equations

$$\rho_M(-i\omega)\tilde{\varphi}_M = \tfrac{1}{3}(2\tilde{g}_{M,\mathrm{s}} + \tilde{g}_{M,\mathrm{d}})\Delta\tilde{\varphi}_M, \tag{4}$$

$$\rho_M(-i\omega)\tilde{\psi}_{M,j} = \tfrac{1}{2}\tilde{g}_{M,\mathrm{s}}\Delta\tilde{\psi}_{M,j}, \quad \text{for } j \in \{x, y, z\}, \tag{5}$$

where $\Delta = \partial_x^2 + \partial_y^2 + \partial_z^2$ is the Laplace operator and the tilde signifies the temporal Fourier transform, then the displacement fields (3) fulfill the linearized momentum conservation equation (1) for a linear, isotropic, homogeneous viscoelastic material with stress-strain relation (2) and without external forces, as appropriate for the surface gravity approximation, as outlined in Appendix B. The densities ρ_M in Eqs. (4) and (5) denote the constant equilibrium densities of the steady-state solution, around which we perturb [22]. To obtain a stable equilibrium around which the linear wave solutions are derived by perturbation, we assume that $\rho_\mathrm{I} \geqslant \rho_\mathrm{III}$, i.e., that the less dense medium is always in the $z > 0$ half-space.

The harmonic wave ansatz [17] consists of choosing the displacement potentials

$$\varphi_M(x, z, t) = \Phi_M \exp\left(-\lambda_{M,\mathrm{l}}^{-1}|z|\right)\exp\left[i(kx - \omega t)\right], \tag{6}$$

$$\psi_{M,j}(x, z, t) = \Psi_M \exp\left(-\lambda_{M,\mathrm{t}}^{-1}|z|\right)\exp\left[i(kx - \omega t)\right]\delta_{jy}, \tag{7}$$

where $j \in \{x, y, z\}$, $M \in \{\mathrm{I}, \mathrm{III}\}$, and we assume the angular frequency $\omega \in \mathbb{R}$ is a given parameter, while the wave number k, the decay lengths $\lambda_{M,\mathrm{l}}$, $\lambda_{M,\mathrm{t}}$, and the coefficients Φ_M, $\Psi_M \in \mathbb{C}$ depend on ω. For $M = \mathrm{I}$ we have $z < 0$, and for $M = \mathrm{III}$ we have $z > 0$, so that the requirement that the displacement decays to zero as $|z| \to \infty$ implies $\mathrm{Re}(\lambda_{M,\mathrm{l}}^{-1})$, $\mathrm{Re}(\lambda_{M,\mathrm{t}}^{-1}) > 0$. Our choice $\omega \in \mathbb{R}$, $k \in \mathbb{C}$ means we consider plane wave solutions with frequency ω, which are damped as they propagate along the x axis, and that we will later solve for $k(\omega)$.

Direct substitution shows that in each half-space, the harmonic wave ansatz fulfills Eqs. (4) and (5) if [22]

$$\lambda_{M,\mathrm{l}}^{-2}(k, \omega) = k^2 + \gamma_M^2(\omega), \tag{8}$$

$$\lambda_{M,\mathrm{t}}^{-2}(k, \omega) = k^2 + \alpha_M^2(\omega), \tag{9}$$

where we define

$$\gamma_M^2(\omega) := \frac{3(-i\omega)\rho_M}{2\tilde{g}_{M,\mathrm{s}}(\omega) + \tilde{g}_{M,\mathrm{d}}(\omega)}, \tag{10}$$

$$\alpha_M^2(\omega) := \frac{2(-i\omega)\rho_M}{\tilde{g}_{M,\mathrm{s}}(\omega)}. \tag{11}$$

Equations (8) and (9) and the requirement $\mathrm{Re}(\lambda_{M,\mathrm{l}}^{-1})$, $\mathrm{Re}(\lambda_{M,\mathrm{t}}^{-1}) > 0$ determine $\lambda_{M,\mathrm{l}}^{-1}$, $\lambda_{M,\mathrm{t}}^{-1}$ uniquely [46]. Physically it makes sense that these decay lengths perpendicular to the interface are fully determined by the bulk properties.

For a given frequency ω, the harmonic wave ansatz then contains five unknowns, namely, k, Φ_I, Ψ_I, Φ_III, Ψ_III. To obtain a dispersion relation $k(\omega)$ we now use the displacement and stress boundary conditions at the interface. Continuity of the two nonvanishing components of the displacement field at $z = 0$, and the stress boundary conditions at $z = 0$, yield a homogeneous linear system of four equations for the four coefficients Φ_I, Ψ_I, Φ_III, and Ψ_III, which is given explicitly in Appendix C. For a propagating wave with nonzero amplitude, this linear system of equations needs to have a nontrivial solution, which means that the determinant of the coefficient matrix must vanish. Equating

this determinant with zero then gives rise to the general dispersion relation

$$
\begin{aligned}
0 = {} & 4\big(k^2\tilde{\Pi}_{2D} + g(\rho_I - \rho_{III}) - \omega^2\rho_{2D}\big)\Big[\big(k^2\tilde{g}_{2D} - i\omega\rho_{2D}\big)\big(k^2 - \lambda_{I,l}^{-1}\lambda_{I,t}^{-1}\big)\big(k^2 - \lambda_{III,l}^{-1}\lambda_{III,t}^{-1}\big) \\
& + i\omega\rho_I\lambda_{I,l}^{-1}\big(k^2 - \lambda_{III,l}^{-1}\lambda_{III,t}^{-1}\big) + i\omega\rho_{III}\lambda_{III,l}^{-1}\big(k^2 - \lambda_{I,l}^{-1}\lambda_{I,t}^{-1}\big)\Big] \\
& + 4\big(k^2\tilde{g}_{2D} - i\omega\rho_{2D}\big)\omega^2\Big[\rho_I\lambda_{I,t}^{-1}\big(k^2 - \lambda_{III,l}^{-1}\lambda_{III,t}^{-1}\big) + \rho_{III}\lambda_{III,t}^{-1}\big(k^2 - \lambda_{I,l}^{-1}\lambda_{I,t}^{-1}\big)\Big] \\
& + \tilde{g}_{I,s}\big(k^2 - \lambda_{III,l}^{-1}\lambda_{III,t}^{-1}\big)\Big[i\omega\tilde{g}_{I,s}\big(-4k^2\lambda_{I,l}^{-1}\lambda_{I,t}^{-1} + \big(k^2 + \lambda_{I,t}^{-2}\big)^2\big) \\
& + 2\rho_{2D}gk^2\big(2\lambda_{I,l}^{-1}\lambda_{I,t}^{-1} - \big(k^2 + \lambda_{I,t}^{-2}\big)\big)\Big] \\
& + \tilde{g}_{III,s}\big(k^2 - \lambda_{I,l}^{-1}\lambda_{I,t}^{-1}\big)\Big[i\omega\tilde{g}_{III,s}\big(-4k^2\lambda_{III,l}^{-1}\lambda_{III,t}^{-1} + \big(k^2 + \lambda_{III,t}^{-2}\big)^2\big) \\
& - 2\rho_{2D}gk^2\big(2\lambda_{III,l}^{-1}\lambda_{III,t}^{-1} - \big(k^2 + \lambda_{III,t}^{-2}\big)\big)\Big] \\
& + (-i\omega)\tilde{g}_{I,s}\tilde{g}_{III,s}\Big[2k^2\big(k^2 + \lambda_{I,t}^{-2}\big)\big(k^2 + \lambda_{III,t}^{-2}\big) + \alpha_I^2\alpha_{III}^2\big(\lambda_{I,t}^{-1}\lambda_{III,l}^{-1} + \lambda_{III,t}^{-1}\lambda_{I,l}^{-1}\big) \\
& + 8k^2\lambda_{I,l}^{-1}\lambda_{I,t}^{-1}\lambda_{III,l}^{-1}\lambda_{III,t}^{-1} - 4k^2\lambda_{I,l}^{-1}\lambda_{I,t}^{-1}\big(k^2 + \lambda_{III,t}^{-2}\big) - 4k^2\lambda_{III,l}^{-1}\lambda_{III,t}^{-1}\big(k^2 + \lambda_{I,t}^{-2}\big)\Big],
\end{aligned}
\tag{12}
$$

where we introduced the in-plane membrane relaxation function

$$
(-i\omega)\tilde{g}_{2D}(\omega) := (-i\omega)(\eta_{2D} + \eta_{2D}') + K_{2D}
\tag{13}
$$

and the out-of-plane membrane relaxation function

$$
\tilde{\Pi}_{2D}(k, \omega) := (-i\omega)\eta_{2D}^{\perp} + \sigma_{2D} + k^2\kappa_{2D},
\tag{14}
$$

where $\eta_{2D}^{\perp}$ denotes the transverse viscosity, which was introduced in Sec. II A. Because η_{2D} and η_{2D}' only appear summed together in Eq. (13), we in the following set $\eta_{2D}' = 0$, with the understanding that η_{2D} includes the effects of both interfacial shear and dilational viscosity.

Equation (12) describes general surface waves at the viscoelastic interface between two viscoelastic bulk fluids and is the main result of this paper. If the effect of gravity is removed, $g = 0$, then the equation becomes symmetric under the interchange of the indices I $\leftrightarrow$ III.

A solution $k(\omega)$ of Eq. (12) represents a surface wave solution; the corresponding phase velocity $c(\omega)$ and propagation distance $\beta^{-1}(\omega)$ are given by

$$
c(\omega) = \frac{\omega}{\text{Re}[k(\omega)]},
\tag{15}
$$

$$
\beta^{-1}(\omega) = \frac{1}{\text{Im}[k(\omega)]}.
\tag{16}
$$

For decaying plane wave solutions that travel in the positive x direction, we are therefore interested in solutions $k(\omega)$ with $\text{Re}[k(\omega)], \text{Im}[k(\omega)] > 0$. For later reference we note that from Eqs. (15) and (16) it follows that if

$$
k \sim \omega^{\nu}
\tag{17}
$$

for some real number ν, then

$$
c \sim \omega^{1-\nu}, \quad \beta^{-1} \sim \omega^{-\nu}.
\tag{18}
$$

As it stands, Eq. (12) is too complicated to allow for general analytic solutions. However, as we discuss in the following sections, and as has been noted for special cases before [8,32,47,48], many known surface wave types can be retrieved from this equation in suitable limits.

C. Factorization of the dispersion relation

If for both bulk media ($M \in \{I, III\}$) the condition [22]

$$
\frac{3\omega\rho_M}{|2\tilde{g}_{M,s}(\omega) + \tilde{g}_{M,d}(\omega)|} \ll |k^2(\omega)| \ll \frac{2\omega\rho_M}{|\tilde{g}_{M,s}(\omega)|}
\tag{19}
$$

holds, and additionally assuming that the gravitational force on the interface can be neglected, i.e.,

$$\rho_{2D}g \ll \omega|\tilde{g}_{M,s}(\omega)|, \qquad M \in \{I, III\}, \tag{20}$$

then Eq. (12) factorizes to

$$0 = [k^2\tilde{\Pi}_{2D} + g(\rho_I - \rho_{III}) - \omega^2(\rho_{2D} + \rho_I\lambda_{I,l} + \rho_{III}\lambda_{III,l})]$$
$$\times [k^2\tilde{g}_{2D} - i\omega(\rho_{2D} + \rho_I\lambda_{I,t} + \rho_{III}\lambda_{III,t})]. \tag{21}$$

By equating either of the two factors with zero, we obtain two independent dispersion relations. Whether a solution $k(\omega)$ of either of the resulting equations fulfills the factorization conditions (19) and (20) can of course only be checked *a posteriori*.

According to Eqs. (8) and (9), in the limit (19) we obtain

$$\lambda_{M,t}^{-2} \approx \alpha_M^2, \quad \lambda_{M,l}^{-2} \approx k^2. \tag{22}$$

Both inequalities in Eq. (19) can be interpreted physically. According to Eqs. (3), (6), and (8), the left inequality implies that $\lambda_{M,l}^{-2} \approx k^2$, so that $\nabla \cdot \boldsymbol{u}_M \approx 0$, which means that the medium is almost incompressible. The right inequality in Eq. (19), on the other hand, can be interpreted physically as a long-wavelength limit. The inequality implies that $\lambda_{M,t}^{-2} \approx \alpha_M^2$ in Eq. (22), which according to Eqs. (7) and (9) means that the decay length of the transversal potential $\boldsymbol{\psi}_M$ away from the interface at $z = 0$ is much smaller than the modulus of the inverse wave number, $1/|k|$, with which the wave propagates along the interface, i.e., $1/|k| \gg |\lambda_{M,t}|$. Since these two interpretations are nonexclusive, wave numbers that satisfy the two inequalities in Eq. (19) describe interfacial wave solutions in the long-wavelength limit surrounded by almost incompressible bulk media.

The first factor in Eq. (21) yields a generalization of the dispersion relation for capillary-gravity-flexural waves on a viscoelastic interface between two unbounded fluids, and can be rearranged as

$$\tilde{\Pi}_{2D}k^2 + (\rho_I - \rho_{III})g = \omega^2(\rho_{2D} + \rho_I\lambda_{I,l} + \rho_{III}\lambda_{III,l}), \tag{23}$$

where $\tilde{\Pi}_{2D}$ is given by Eq. (14). Using Eq. (14), assuming the bending rigidity in $\tilde{\Pi}_{2D}$ is negligible, a crossover from surface-tension driven waves to a transverse-viscosity dominated response occurs at the frequency

$$\omega_{2D}^{\sigma} \equiv \frac{\sigma_{2D}}{\eta_{2D}^{\perp}}. \tag{24}$$

We give a physical interpretation of Eq. (23) by observing that the equation formally looks similar to a Fourier transformed wave equation with additional restoring force. This becomes more obvious upon rewriting the equation as

$$\tilde{\Pi}_{2D}(ik)^2 - (\rho_I - \rho_{III})g = (-i\omega)^2(\rho_{2D} + \rho_I\lambda_{I,l} + \rho_{III}\lambda_{III,l}). \tag{25}$$

The right-hand side contains a factor $(-i\omega)^2$, which represents a second temporal derivative and hence describes an acceleration. The effective area mass density which couples to this inertia is given by the sum of the surface excess mass area density ρ_{2D} and the effective area mass densities associated with the longitudinal part of the wave, $\rho_I\lambda_{I,l}$ and $\rho_{III}\lambda_{III,l}$, respectively. To see this, we note that according to Eq. (6), $\lambda_{M,l}$ represents the penetration depth of the longitudinal part of the wave into bulk medium M, so that $\rho_M\lambda_{M,l}$ is the effective area mass density of the longitudinal oscillation in medium M. That the longitudinal part of the displacement is dominant for capillary-gravity-flexural waves is plausible, as for inviscid incompressible Euler flow the capillary-gravity dispersion relation can be derived assuming only a longitudinal displacement field [3]. The inertia term in Eq. (25) is balanced by a linear restoring force, with strength $(\rho_I - \rho_{III})g$, and a force coupling to the surface deformation, represented by $\tilde{\Pi}_{2D}(ik)^2$. According to Eq. (14), this force has elastic, dissipative, and bending, components. Performing an inverse Fourier transform of Eq. (25) is not straightforward, for two reasons. First, $\lambda_{M,l}$ depends on both k and ω via a complex square

root, so that it in general does not correspond to a simple spatial or temporal derivative in real space. Second, since we here derive the dispersion relation via the harmonic wave ansatz, the physical interpretation of the function that obeys the inverse-Fourier-transformed Eq. (25) is not obvious. From comparing the dispersion relation (25) with the stress tensor boundary conditions for the surface displacement in the z direction, which is given in Appendix C, it is plausible that Eq. (25) is the Fourier transformed equation of motion for the surface displacement in the z direction; however, showing this rigorously is beyond the scope of the current work.

The second factor in Eq. (21) corresponds to a generalization of the Lucassen dispersion relation [10,12] and results in

$$k^2 = \frac{i\omega}{\tilde{g}_{2D}}(\rho_{2D} + \rho_I \lambda_{I,t} + \rho_{III} \lambda_{III,t}), \tag{26}$$

where $\tilde{g}_{2D}$ is defined in Eq. (13). This equation also has a physical interpretation in terms of a force balance equation [16]. To see this, we first rewrite the dispersion relation as

$$-i\omega(ik)^2 \tilde{g}_{2D} = (-i\omega)^2 (\rho_{2D} + \rho_I \lambda_{I,t} + \rho_{III} \lambda_{III,t}). \tag{27}$$

For a half-space filled with an incompressible Newtonian fluid, and bounded by a purely elastic membrane, it has been shown that Eq. (27) describes the interfacial displacement in the x direction, so that the equation describes a compression wave. Furthermore, for the Newtonian-fluid model the inverse Fourier transform has been carried out explicitly, to derive a fractional wave equation [16]. We here recall the interpretation of Eq. (27) as equation of motion for the in-plane interface displacement: The right-hand side has a factor $(-i\omega)^2$, and hence corresponds to the acceleration of the interface. The effective area mass density relevant for this inertia term consists of three contributions, namely the surface excess mass area density ρ_{2D}, and the effective area mass density of the bulk media oscillating above and below the interface, which for the Lucassen wave is dominated by the transversal motion and hence given by $\rho_I \lambda_{I,t}$ and $\rho_{III} \lambda_{III,t}$. The penetration depth of the wave into the bulk medium, $\lambda_{M,t}$, in general depends on the angular frequency ω, so that the effective area mass density becomes frequency-dependent. Because of this, it is not possible to explicitly perform the inverse Fourier transform of Eq. (27) without specifying the viscoelastic response of the bulk media. The left-hand side of Eq. (27) describes the force with which the interface responds to local compression along the interface, as described by the factor $(ik)^2$. Using Eq. (13) the prefactor becomes $-i\omega\tilde{g}_{2D}(\omega) = (-i\omega)\eta_{2D} + K_{2D}$, so that local compression of the interface leads to both an elastic response, described by K_{2D}, and dissipation, described by η_{2D}.

The generalized Lucassen dispersion relation (27) gives rise to several crossover frequencies. Whether for a given frequency the inertia term is dominated by the bulk media or the interface can be estimated by comparing ρ_{2D} with $\rho_I|\lambda_{I,t}| + \rho_{III}|\lambda_{III,t}|$. By equating these two expressions, and using $\lambda_{M,t}^{-1} \approx \alpha_M$ together with Eq. (11), we obtain the corresponding crossover frequency ω_{2D}^ρ as solution of the equation

$$\frac{\sqrt{\rho_I |\tilde{g}_{I,s}(\omega_{2D}^\rho)|} + \sqrt{\rho_{III} |\tilde{g}_{III,s}(\omega_{2D}^\rho)|}}{\sqrt{2\omega_{2D}^\rho}} = \rho_{2D}, \tag{28}$$

where both $\tilde{g}_{I,s}$, $\tilde{g}_{III,s}$ are evaluated at ω_{2D}^ρ. If the expression on the left-hand side of this equation, when evaluated at an angular frequency ω, is much larger than the expression on the right-hand side, inertia effects of the bulk media dominate over those of the interface, and vice versa. Similarly, whether the response of the membrane to compression is dominated by elasticity or viscosity switches at the crossover frequency

$$\omega_{2D}^{\text{elastic}} \equiv \frac{K_{2D}}{\eta_{2D}}. \tag{29}$$

For $\omega \ll \omega_{2D}^{\text{elastic}}$, the membrane response is predominantly elastic, whereas for $\omega \gg \omega_{2D}^{\text{elastic}}$, viscous dissipation dominates.

We remark that $\lambda_{M,\mathrm{l}}$ and the bending properties $\kappa_{2\mathrm{D}}$ and $\eta_{2\mathrm{D}}^{\perp}$ (which are contained in $\tilde{\Pi}_{2\mathrm{D}}$) only enter the dispersion relation (23), while $\lambda_{M,\mathrm{t}}$ and the in-plane viscoelastic response of the surface, described by $\eta_{2\mathrm{D}}$, $K_{2\mathrm{D}}$ (which are contained in $\tilde{g}_{2\mathrm{D}}$), only enter Eq. (26). This is consistent with the picture of the capillary-gravity-flexural wave as a transversal wave which contains significant out-of-plane deformation, and the Lucassen wave as a pressure wave in the interface which is dominated by the displacement in the plane of the interface [16].

The factorization Eq. (21) generalizes previous factorizations derived for an interface at a fluid half-space [22,32,47]. That a factorization like Eq. (21) does not always hold for physically relevant parameters was already predicted by Lucassen [47], and in the context of a fluid half-space is an established experimental result [8,48]. Equation (12) therefore contains more information as compared to Eq. (21), as the full dispersion relation allows to infer the range of validity of each limiting case, as well as the interrelations between the limiting cases.

III. ANALYTICAL LIMITING CASES

A. Symmetric scenario

We now assume that media I and III have the same properties, i.e., that $\rho \equiv \rho_{\mathrm{I}} = \rho_{\mathrm{III}}$, $\tilde{g}_{\mathrm{s}} \equiv \tilde{g}_{\mathrm{I,s}} = \tilde{g}_{\mathrm{III,s}}$, $\tilde{g}_{\mathrm{d}} \equiv \tilde{g}_{\mathrm{I,d}} = \tilde{g}_{\mathrm{III,d}}$, so that $\alpha \equiv \alpha_{\mathrm{I}} = \alpha_{\mathrm{III}}$, $\lambda_{\mathrm{l}} \equiv \lambda_{\mathrm{I,l}} = \lambda_{\mathrm{III,l}}$, $\lambda_{\mathrm{t}} \equiv \lambda_{\mathrm{I,t}} = \lambda_{\mathrm{III,t}}$. In this case, the dispersion relation (12) simplifies to

$$0 = (k^2 \tilde{\Pi}_{2\mathrm{D}} - \omega^2 \rho_{2\mathrm{D}})\big(k^2 - \lambda_{\mathrm{l}}^{-1}\lambda_{\mathrm{t}}^{-1}\big)\big[(k^2 \tilde{g}_{2\mathrm{D}} - i\omega\rho_{2\mathrm{D}})\big(k^2 - \lambda_{\mathrm{l}}^{-1}\lambda_{\mathrm{t}}^{-1}\big) + 2i\omega\rho\lambda_{\mathrm{l}}^{-1}\big]$$
$$+ 2\omega^2 \rho \lambda_{\mathrm{t}}^{-1}(k^2 \tilde{g}_{2\mathrm{D}} - i\omega\rho_{2\mathrm{D}})\big(k^2 - \lambda_{\mathrm{l}}^{-1}\lambda_{\mathrm{t}}^{-1}\big) - \tfrac{1}{2}i\omega\tilde{g}_{\mathrm{s}}^2\lambda_{\mathrm{l}}^{-1}\lambda_{\mathrm{t}}^{-1}\big[\alpha^4 + \big(k^2 - \lambda_{\mathrm{t}}^{-2}\big)^2\big], \quad (30)$$

which also factorizes under the assumptions (19) and (20) to yield

$$0 = [k^2 \tilde{\Pi}_{2\mathrm{D}} - \omega^2(\rho_{2\mathrm{D}} + 2\rho\lambda_{\mathrm{l}})][k^2 \tilde{g}_{2\mathrm{D}} - i\omega(\rho_{2\mathrm{D}} + 2\rho\lambda_{\mathrm{t}})]. \tag{31}$$

This equation follows alternatively from the previous factorization (21), and shows that in the symmetric scenario gravitational acceleration becomes irrelevant. Equating each of the two factors in Eq. (31) with zero yields generalizations of the well-known capillary and Lucassen waves at interfaces separating two identical media [3,10].

B. Asymmetric scenario

We now consider the asymmetric case, where medium III can be neglected in comparison to medium I. Typically, this is the case when medium I is much denser than medium III. The dispersion relation for this case has been derived before [22] and proceeds similar to Sec. II, but without explicitly taking into account the displacement above the interface, $z > 0$. The resulting equation is [22]

$$0 = 4(k^2 \tilde{\Pi}_{2\mathrm{D}} + \rho_{\mathrm{I}}g - \omega^2 \rho_{2\mathrm{D}})\big[(k^2 \tilde{g}_{2\mathrm{D}} - i\omega\rho_{2\mathrm{D}})\big(k^2 - \lambda_{\mathrm{I,l}}^{-1}\lambda_{\mathrm{I,t}}^{-1}\big) + i\omega\rho_{\mathrm{I}}\lambda_{\mathrm{I,l}}^{-1}\big]$$
$$+ 4(k^2 \tilde{g}_{2\mathrm{D}} - i\omega\rho_{2\mathrm{D}})\omega^2 \rho_{\mathrm{I}}\lambda_{\mathrm{I,t}}^{-1} + \tilde{g}_{\mathrm{I,s}}\big\{i\omega\tilde{g}_{\mathrm{I,s}}\big[-4k^2\lambda_{\mathrm{I,l}}^{-1}\lambda_{\mathrm{I,t}}^{-1} + \big(k^2 + \lambda_{\mathrm{I,t}}^{-2}\big)^2\big]$$
$$+ 2\rho_{2\mathrm{D}}gk^2\big[2\lambda_{\mathrm{I,l}}^{-1}\lambda_{\mathrm{I,t}}^{-1} - \big(k^2 + \lambda_{\mathrm{I,t}}^{-2}\big)\big]\big\}. \tag{32}$$

This equation also follows from the full dispersion relation (12) in the limit

$$\frac{\rho_{\mathrm{III}}}{\rho_{\mathrm{I}}} \ll 1, \quad |\lambda_{\mathrm{III,l}}k| \approx 1, \quad |\lambda_{\mathrm{III,t}}| \lesssim |\lambda_{\mathrm{I,t}}|, \tag{33}$$

where $|\lambda_{\mathrm{III,l}}k| \approx 1$ is obeyed for a medium III that is almost incompressible.

We now give a short summary of the waves described by Eq. (32), and refer the reader to Ref. [22] for more details.

Upon removing the effects related to the surface ($\rho_{2D} = 0$, $\tilde{g}_{2D} = 0$, $\tilde{\Pi}_{2D} = 0$) and also gravity ($g = 0$), Eq. (32) becomes

$$4k^2 \lambda_{\mathrm{I,l}}^{-1} \lambda_{\mathrm{I,t}}^{-1} = \left(k^2 + \lambda_{\mathrm{I,t}}^{-2}\right)^2, \tag{34}$$

where $\lambda_{\mathrm{I,l}}^{-1}$, $\lambda_{\mathrm{I,t}}^{-1}$ are given by Eqs. (8) and (9). This is the classical Rayleigh conditional equation [17] whose solutions lead to the known (viscoelastic) Rayleigh waves [18,19]. For a viscoelastic bulk material Eq. (34) has two distinct solutions $k(\omega)$ [18,19]. In particular, there are two distinct solutions to Eq. (34) for the vacuum-water interface, which are shown in Fig. 7 in Appendix D.

Similarly to Sec. II C, the conditional equation (32) factorizes if the inequalities (19) and (20) hold for the half-space. Equation (32) then becomes

$$0 = [k^2 \tilde{\Pi}_{2D} + \rho_{\mathrm{I}} g - \omega^2 (\rho_{2D} + \rho_{\mathrm{I}} \lambda_{\mathrm{I,l}})][k^2 \tilde{g}_{2D} - i\omega(\rho_{2D} + \rho_{\mathrm{I}} \lambda_{\mathrm{I,t}})], \tag{35}$$

which equivalently follows from Eq. (21) in the limit (33). By equating each of the factors of Eq. (35) with zero, we obtain two equations which correspond to two different wave solutions [22]. The first factor yields a generalization of the capillary-gravity-flexural surface wave, the second a generalization of the Lucassen wave. As has been shown before, for high frequencies the factorization (35) can break down, and a frequency-dependent transition from the Lucassen wave to a Rayleigh wave can occur [22].

For an incompressible Newtonian fluid, the second factor in Eq. (35), which corresponds to the Lucassen wave solution, has been shown to be the Fourier transform of a fractional wave equation [16]. Using a simplified system that describes interfacial pressure waves in elastic monolayers at the water-air interface via coupling a one-dimensional wave equation, representing the dynamics of the interface, to a parabolic equation on the half-space below, a mathematically rigorous limit leading to a fractional wave equation is presented in Ref. [49].

C. Free membrane

To obtain the dispersion relation for a free membrane in vacuum, we consider a limit of Eq. (32) in which medium I is negligible compared to the interface. This is the case if

$$\frac{\rho_{\mathrm{I}} \lambda_{\mathrm{I,t}}}{\rho_{2D}} \ll 1, \qquad \frac{\rho_{\mathrm{I}} \lambda_{\mathrm{I,l}}}{\rho_{2D}} \ll 1, \tag{36}$$

which means that the oscillating mass of the motion below the membrane is negligible compared to the membrane surface excess mass area density. The conditional equation (32) then factorizes as

$$0 = (k^2 \tilde{\Pi}_{2D} - \omega^2 \rho_{2D})(k^2 \tilde{g}_{2D} - i\omega \rho_{2D}), \tag{37}$$

which is alternatively obtained from Eq. (35) in the limit (36).

Equating the first factor in Eq. (37), which comes from the capillary wave factor in Eq. (35), with zero and substituting the definition of $\tilde{\Pi}_{2D}$, Eq. (14), yields

$$-\kappa_{2D}(-ik)^4 + \eta_{2D}^{\perp}(-i\omega)(-ik)^2 + \sigma_{2D}(-ik)^2 = \rho_{2D}(-i\omega)^2, \tag{38}$$

which is a generalization of the classical dispersion relation of a bending wave in an elastic plate [40], recovered in the limit $\eta_{2D}^{\perp} = 0$, $\sigma_{2D} = 0$. If the first factor of Eq. (37) is equal to zero, it can be seen directly from the system of equations used to derive the general dispersion relation in Appendix C that $\Phi = 0$ in Eq. (6), so that the displacement field $\boldsymbol{u}$ corresponding to the dispersion relation (38) is purely transversal.

Using the definition of $\tilde{g}_{2D}$, Eq. (13), and equating the second factor of Eq. (37) with zero, yields a one-dimensional wave equation

$$(-ik)^2 K_{2D} + (-i\omega)(-ik)^2 \eta_{2D} = (-i\omega)^2 \rho_{2D}. \tag{39}$$

If Eq. (39) holds, it can be seen from the system of equations used to derive the general dispersion relation in Appendix C that $\Psi = 0$ in Eq. (7), so that the displacement field $\boldsymbol{u}$ is purely longitudinal.

Thus, while in general both the longitudinal and transversal displacements in Eq. (3) are necessary to fulfill momentum conservation and the boundary conditions, for a membrane in vacuum the two fields decouple.

IV. EXAMPLE SYSTEMS

A. Newtonian fluid as bulk medium

1. Viscoelastic relaxation functions for compressible Newtonian fluid

To apply our theory to situations where water is at least one of the bulk media and gravity is present, we need to relate the viscoelastic stress-strain relation (2) to the usual stress-strain relation for a compressible Newtonian fluid. This is done by including gravity, modeled as an external force $F_{M,i} = -\delta_{iz}\rho_M g$, into the argumentation usually carried out to derive sound waves in bulk media [3,4,45], see Ref. [22] for more details. For a compressible Newtonian fluid, the shear and dilational relaxation functions follow as

$$\tilde{g}_{M,\mathrm{s}} = 2\eta_M, \tag{40}$$

$$\tilde{g}_{M,\mathrm{d}}(\omega) = 3\eta'_M + \frac{3K_M}{-i\omega}, \tag{41}$$

where η_M, η'_M are the shear- and dilational viscosity of medium M, and K_M is the modulus of compression (bulk modulus) of the fluid, which for adiabatic compression is related to the sound velocity c_M as $K_M = \rho_M c_M^2$ [3]. The relaxation function (41) describes the response of a Kelvin-Voigt material and switches from a predominantly elastic to a viscous response if ω exceeds the crossover frequency

$$\omega_{M,\mathrm{d}} \equiv \frac{K_M}{\eta'_M}. \tag{42}$$

For the effect of gravity, we use the surface gravity approximation [45], for which effects of gravity only enter in the boundary conditions at $z = 0$; cf. Appendix C.

If the Newtonian fluid is weakly compressible, such that $\eta_M, \eta'_M \ll 3K_M/\omega$, then the factorization conditions (19) become

$$\frac{K_M}{3\omega} \gg \frac{\omega\rho_M}{|k|^2} \gg \frac{\eta_M}{2}. \tag{43}$$

Substituting the relaxation functions (40) and (41), into the generalized capillary-gravity-flexural dispersion relation (23), we obtain

$$\tilde{\Pi}_{2\mathrm{D}}k^2 = \omega^2\left(\frac{\rho_\mathrm{I} + \rho_\mathrm{III}}{k} + \rho_{2\mathrm{D}}\right) - (\rho_\mathrm{I} - \rho_\mathrm{III})g, \tag{44}$$

where we use that $\lambda_{M,\mathrm{l}}^{-1} \approx k$ holds in the limit (43). If $\tilde{\Pi}_{2\mathrm{D}} \approx \sigma_{2\mathrm{D}}$, then Eq. (44) is the classical dispersion relation for capillary-gravity waves for Newtonian fluids [50].

On the other hand, the Lucassen dispersion relation (26) yields

$$k^2 = \frac{i\omega}{\tilde{g}_{2\mathrm{D}}}\left(\sqrt{\frac{\rho_\mathrm{I}\eta_\mathrm{I}}{-i\omega}} + \sqrt{\frac{\rho_\mathrm{III}\eta_\mathrm{III}}{-i\omega}} + \rho_{2\mathrm{D}}\right), \tag{45}$$

where we use that $\lambda_{M,\mathrm{t}}^{-1} \approx (-i\omega\rho_M/\eta_M)^{1/2}$ holds in the limit (43). Substituting the definition of $\tilde{g}_{2\mathrm{D}}$ (13) into Eq. (45), we obtain

$$k = \sqrt{\frac{\rho_{2\mathrm{D}}\omega^2 + e^{i\pi/4}\left(\sqrt{\rho_\mathrm{I}\eta_\mathrm{I}\omega^3} + \sqrt{\rho_\mathrm{III}\eta_\mathrm{III}\omega^3}\right)}{K_{2\mathrm{D}} - i\omega\eta_{2\mathrm{D}}}}, \tag{46}$$

where we have chosen the complex square root that leads to a positive real part for k, so that the resulting wave propagates in the positive x direction. This is a generalization of the Lucassen dispersion relation [9–12], which was originally derived for a half-space filled with an incompressible Newtonian fluid, and without taking into account interfacial inertia. Upon neglecting the membrane viscosity, $\eta_{2D} = 0$, Eq. (46) reduces to one central result from Ref. [35], where the Lucassen wave was discussed for elastic interfaces separating two Newtonian fluids.

For future reference, we note that for the Lucassen wave on a Newtonian fluid, the crossover frequency at which the interfacial inertia dominates over the bulk fluid inertia is obtained by substituting the shear relaxation function (40) into Eq. (28), which yields

$$\omega_{2D}^{\rho} = \left(\frac{\sqrt{\rho_I \eta_I} + \sqrt{\rho_{III} \eta_{III}}}{\rho_{2D}} \right)^2. \tag{47}$$

For angular frequencies above ω_{2D}^{ρ}, the Lucassen wave behaves thus like the one-dimensional wave equation solution for a free membrane, Eq. (39). This will be used to estimate crossover frequencies in Secs. IV A 2, IV A 3, IV B 1, and IV B 2.

2. Water-water interface

The Newtonian fluid model deserves further attention, since water, which is ubiquitous and fundamentally important for life on earth, is very well described as a Newtonian fluid up to angular frequencies slightly below the THz regime [42,51–53], as we discuss further below.

We consider water at 25 °C for media I and III, and use the parameters [54] $\eta \approx 1 \times 10^{-3}$ Pa s, $\eta' \approx 3 \times 10^{-3}$ Pa s, $\rho \approx 1 \times 10^3$ kg/m^3, $c \approx 1.5 \times 10^3$ m/s. For the interface, we use the parameters $g = 9.81$ m/s^2, $\rho_{2D} = 1 \times 10^{-6}$ kg/m^2, $\eta_{2D} = 1 \times 10^{-9}$ Pa s m, $\eta'_{2D} = 0$, $\eta_{2D}^{\perp} = 1 \times 10^{-9}$ Pa s m, $K_{2D} = 34 \times 10^{-3}$ N/m, $\sigma_{2D} = 5 \times 10^{-3}$ N/m, $\kappa_{2D} = 3 \times 10^{-19}$ N m, appropriate for a planar DPPC bilayer immersed in water. The values for σ_{2D} and K_{2D} are obtained for monolayers via measuring Langmuir isotherms [14,55], the shear viscosity η_{2D} for a DPPC bilayer is estimated from measurements of diffusing lipids in lipid membranes [56,57], while the bending rigidity κ_{2D} is extracted from weakly deforming bilayer vesicles [58,59]. Although the values for σ_{2D} and K_{2D} are obtained for monolayers, we assume for our numerical study that the corresponding values for a bilayer are comparable. For the transverse membrane viscosity $\eta_{2D}^{\perp}$, we did not find any experimentally measured values for a DPPC membrane in the literature; we therefore use the same value as for η_{2D}. For Langmuir monolayers in a trough, the surface excess mass area density ρ_{2D} can be calculated as the quotient of added lipid mass and trough area. We use a typical value for DPPC monolayers in the context of surface wave measurements [14].

The Newtonian fluid model (40) and (41) describes bulk water in a limited frequency range and starts to break down on timescales comparable to those of the individual water molecule dynamics [42,51–53]. For example, the shear response starts to deviate from Eq. (40) on the timescale of water molecule rearrangements in the hydrogen bond network, corresponding to frequencies $\omega \gtrsim 10^{11}$ s^{-1} [42,51–53]; similar effects are expected for the dilational response. In fact, as we will see below, the dilational crossover frequency (42) is of the order of 10^{11} s^{-1} for water. Likewise, for molecular length scales we expect that the assumption of a homogeneous medium will break down [51], and that the dependence of the fluid response on the distance from the interface will become relevant [60]. Therefore, while our analysis below extends to angular frequencies $\omega = 10^{14}$ s^{-1}, the high-frequency range $\omega = 10^{11}$ s^{-1} to $\omega = 10^{14}$ s^{-1} is included primarily to study the mathematical behavior of the dispersion relation, and is not expected to accurately describe the response of actual water in an experimental system. To put these high frequencies into perspective, we note that in experiments usually lower frequencies are considered. For example, Ref. [48] observed thermally excited capillary waves on the free surface of water via laser light scattering for angular frequencies of $\omega \approx 10^6$ s^{-1}. In Ref. [13] sound waves on lipid monolayers were measured for angular frequencies of up to $\omega \approx 10^7$ s^{-1}. There exist, however, bulk experiments that probe the non-Newtonian response of water at $\omega \approx 10^{11}$ s^{-1} without an interface present [52]. Note that
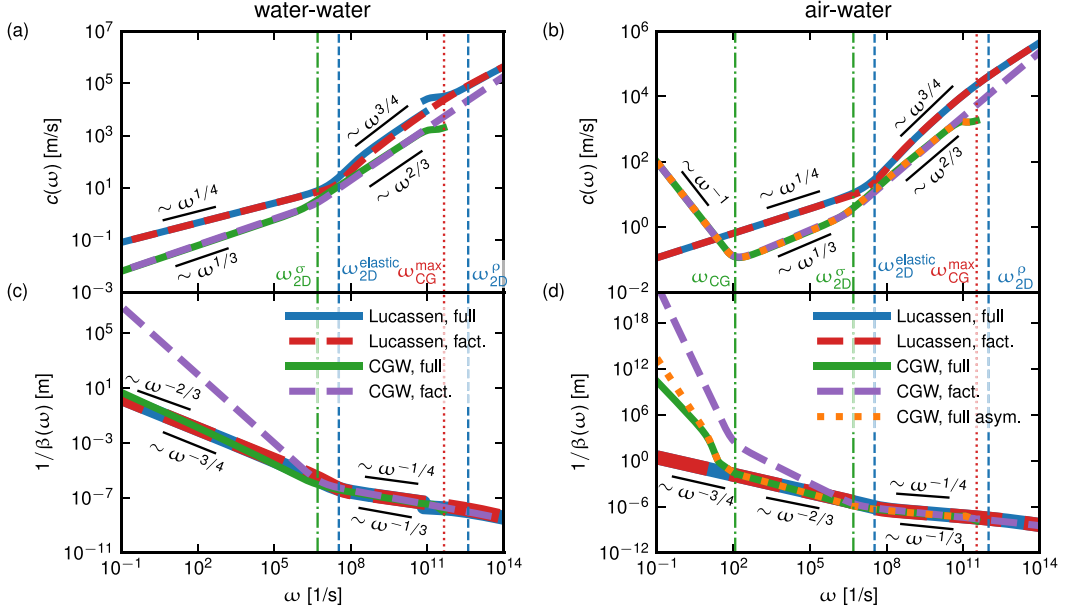
FIG. 2. (a, c) Properties of waves at an interface separating two Newtonian fluids with identical parameters, as discussed in Sec. IV A 2. Parameters are given in Sec. IV A, and correspond to a DPPC membrane (interface) and water (bulk). The full dispersion relation (30) (solid blue and green lines) and the equations that correspond to the individual factors of the factorized symmetric dispersion relation (31), i.e., Eqs. (44) (dashed purple line) and (45) (dashed red line), are solved numerically to obtain the wave number k as a function of ω. The corresponding (a) phase velocity and (c) propagation distance are then calculated using Eqs. (15) and (16). (b, d) Phase velocities and propagation distances for an air-water interface, as discussed in Sec. IV A 3. Both the full dispersion relation (12) (solid blue and green lines) and the equations corresponding to the individual factors of the factorized asymmetric dispersion relation (35) (dashed red and purple lines) are solved numerically, and the resulting wave number $k(\omega)$ is used to calculate c, β^{-1} via Eqs. (15) and (16). Additionally, the solution of the asymmetric vacuum-water dispersion relation (32) is shown for comparison (dotted orange line). For all subplots, vertical dashed lines denote the various crossover frequencies discussed for (a) and (c) in Sec. IV A 2 and for (b) and (d) in Sec. IV A 3; green dash-dotted lines denote crossovers in the capillary-gravity-flexural wave (CGW), and blue dashed lines indicate crossovers in the Lucassen wave. Red dotted lines highlight the frequencies at which solutions of the full dispersion relation disappear. The power-law scalings of c and β^{-1} within each scaling regime are indicated by black bars.

by using the viscoelastic response functions published in Ref. [42], it is possible to include the non-Newtonian high-frequency response of bulk water into our theory; however, this is out of the scope of the present work.

We numerically solve the full dispersion relation (12), which is equivalent to Eq. (30) in the symmetric case, as well as the factorization (31) for k for a wide range of frequencies ω. By comparing whether a solution of the factorized equation agrees with the respective solutions of the full equation, we can assess whether the factorization (31) holds for our particular choice of materials. For the two distinct solutions for $k(\omega)$ that we find, we calculate the phase velocities and propagation distances via Eqs. (15) and (16). In Figs. 2(a) and 2(c) we compare the results to phase velocities and propagation distances obtained from numerical solutions of the factorized dispersion relation, Eq. (31), which for a Newtonian fluid are given by Eqs. (44) and (45) with $\rho \equiv \rho_{\mathrm{I}} = \rho_{\mathrm{III}}$, $\eta \equiv \eta_{\mathrm{I}} = \eta_{\mathrm{III}}$.

The phase velocity of one numerical solution of the full dispersion relation (30) agrees with the capillary-gravity-flexural wave (CGW) dispersion relation (44) for most of the frequency range

considered. For angular frequencies $\omega \ll 10^7 \, \text{s}^{-1}$, the bulk inertia dominates over the interfacial inertia in Eq. (44), so that $k^3 \approx 2\omega^2 \rho/\sigma_{2D}$, where we use that for the frequencies and wave numbers in that regime it holds that $\tilde{\Pi}_{2D} \approx \sigma_{2D}$. This approximate expression for k implies $k \sim \omega^{2/3}$, and consequently $c = \omega/k \sim \omega^{1/3}$, as observed in the figure. According to Eq. (24), at the crossover frequency $\omega_{2D}^\sigma \equiv \sigma_{2D}/\eta_{2D}^\perp = 5 \times 10^6 \, \text{s}^{-1}$, the viscous dissipation term in the interfacial response $\tilde{\Pi}_{2D}$ starts to dominate over the surface tension, so that $\tilde{\Pi}_{2D} \approx -i\omega\eta_{2D}^\perp$. The right-hand side of Eq. (44) is still dominated by the bulk inertia, so that $k \sim \omega^{1/3}$, and hence $c \sim \omega^{2/3}$, as indicated in Fig. 2(a) by a black bar. Finally, at $\omega_d \equiv K/\eta' = 5 \times 10^{11} \, \text{s}^{-1}$, the dilational viscosity starts to dominate over the elastic response in Eq. (41); the compressibility of the fluid starts to become more relevant, and the solution corresponding to the capillary-flexural wave seizes to exist at $\omega_{CG}^{max} \approx 3.4 \times 10^{11} \, \text{s}^{-1}$. While this breakdown of the capillary-flexural wave is an interesting mathematical fact, we emphasize again that at frequencies in the THz regime, the assumption that water behaves as a Newtonian fluid breaks down, and Eqs. (40) and (41) need to be amended to obtain a physically accurate description of the viscoelastic properties of water at such high frequencies [42,51–53]. The phase velocity of the second solution of Eq. (30) agrees with the Lucassen wave dispersion relation (45) almost perfectly throughout the frequency range considered, except for a discontinuity at the frequency $\omega_d = 5 \times 10^{11} \, \text{s}^{-1}$, where the dilational bulk response switches from elasticity dominated to viscous. The crossover frequencies (29) and (47), associated with the Lucassen wave are given by $\omega_{2D}^\rho = 4 \times 10^{12} \, \text{s}^{-1}$, $\omega_{2D}^{elastic} = 3.4 \times 10^7 \, \text{s}^{-1}$. For frequencies $\omega \ll \omega_{2D}^{elastic}$, the Lucassen wave dispersion relation is thus approximately given by $K_{2D}k^2 \approx 2e^{i\pi/4}\sqrt{\rho\eta\omega^3}$, so that $k \sim \omega^{3/4}$ and hence $c \sim \omega^{1/4}$, as shown by a black bar in Fig. 2(a). At the crossover frequency $\omega_{2D}^{elastic}$, the interfacial viscosity starts to dominate over the interfacial elasticity, so that $-i\omega\eta_{2D}k^2 \approx 2e^{i\pi/4}\sqrt{\rho\eta\omega^3}$, and hence $k \sim \omega^{1/4}$, which implies $c \sim \omega^{3/4}$, as observed approximately in Fig. 2(a). The slight deviations from the expected scaling might indicate that the factorization condition does not hold perfectly in this regime. For very large frequencies $\omega \gg \omega_{2D}^\rho$, the Lucassen dispersion relation approximately yields $k^2 \approx i\omega\rho_{2D}/\eta_{2D}$, meaning $k \sim \omega^{1/2}$ from which we obtain $c \sim \omega^{1/2}$. The onset of this regime can be observed in Figs. 2(a) and 2(c) at the highest frequencies shown.

In Fig. 2(c) we show the propagation distances β^{-1}, defined in Eq. (16), corresponding to the solutions of both the full and factorized dispersion relations; we calculate the propagation distances using the same complex wave numbers $k(\omega)$ as used for Fig. 2(a). Overall, both the factorized capillary-flexural wave and the Lucassen wave propagation distances agree with the full solution, and show scalings fully consistent with Eqs. (17) and (18) and the local scalings of k with ω discussed in the context of Fig. 2(a). The only exception to this is the low-frequency regime of the capillary-gravity-flexural wave, where the factorized dispersion relation (44) predicts a propagation distance orders of magnitude larger as compared to the full dispersion relation (30). Furthermore, the expected scaling of $\beta^{-1} \sim \omega^{-2/3}$ for the capillary-gravity-flexural wave for angular frequencies $\omega \ll 10^7 \, \text{s}^{-1}$ does not fit perfectly to the prediction of Eq. (30), so that real and imaginary parts of $k(\omega)$ scale differently with ω in this regime. This shows that while the factorized dispersion relation (44) captures the real part of the wave number properly, for the imaginary part the full dispersion relation is necessary.

We show example displacement plots of a Lucassen and capillary-gravity-flexural wave (CGW) at $\omega \approx 10^3 \, \text{s}^{-1}$ in Figs. 3(a) and 3(c), respectively. The displacement plots are generated by solving Eq. (30) for $k(\omega)$ to obtain the displacement potentials ϕ, $\boldsymbol{\psi}$ via Eqs. (6) and (7). The displacement field is then obtained via Eq. (3). In Fig. 3 all displacement fields are shown for frequencies lower than the first crossover frequencies in Fig. 2, i.e., in the elastic regime for the Lucassen wave and in the surface-tension-driven regime for the capillary-gravity-flexural wave, respectively. Displacements at frequencies higher than the first crossover frequency are shown in Fig. 8 in Appendix E. In all plots, the displacements of the bulk media are shown as blue and red colored grids, representing water and air, respectively. The interface is shown as a green line. We include the dominant decay lengths of the wave as well as trajectories of single volume elements in black. Note that in the harmonic wave ansatz the displacement is translationally invariant in the y coordinate
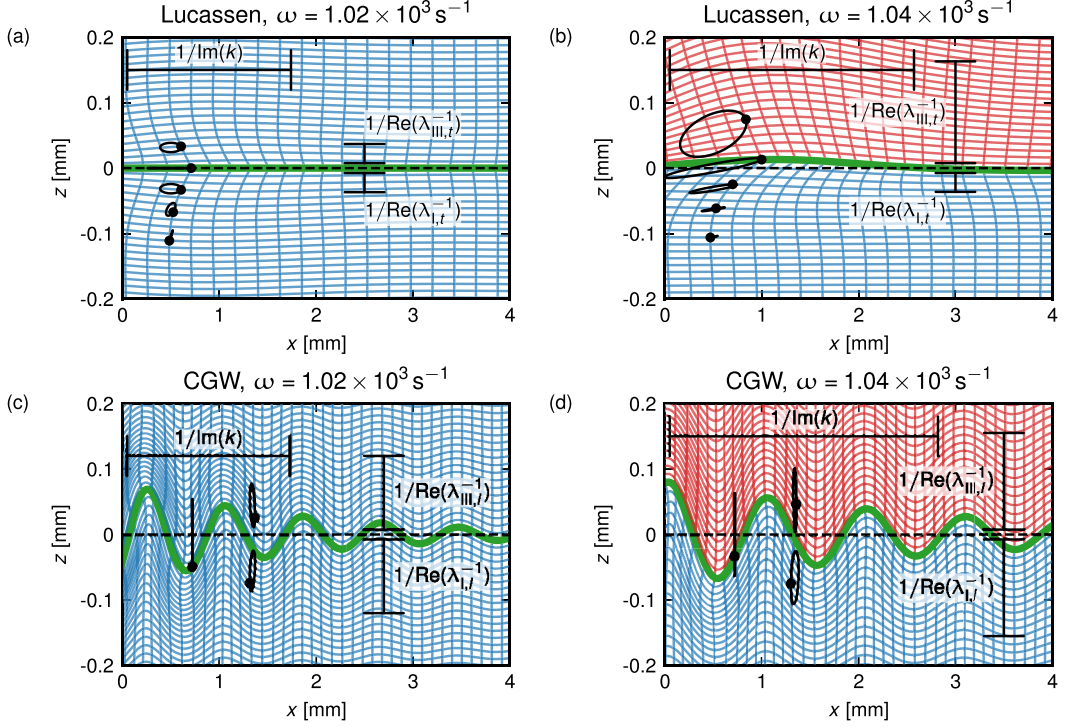
FIG. 3. Plots of the displacement field $\boldsymbol{u}(\boldsymbol{r}, t)$ of Lucassen and capillary-gravity-flexural waves (CGW) in the elastic and surface-tension-dominated regime, respectively. The scaling is chosen such that the respective dominant decay lengths into the bulk media, $1/\mathrm{Re}(\lambda_{M,t}^{-1})$ and $1/\mathrm{Re}(\lambda_{M,l}^{-1})$, as well as the propagation distance $\beta^{-1} = 1/\mathrm{Im}(k)$ are well visible in the plot. The displacement of the interface is shown as a green line. Bulk water displacement is shown as a blue grid, whereas bulk air displacement is shown as a red grid. Decay lengths and volume element trajectories are shown in black. (a) Lucassen wave at water-water interface with $\omega = 1.02 \times 10^3\,\mathrm{s}^{-1}$. (b) Lucassen wave at air-water interface with $\omega = 1.04 \times 10^3\,\mathrm{s}^{-1}$. (c) Capillary-gravity-flexural wave at water-water interface with $\omega = 1.02 \times 10^3\,\mathrm{s}^{-1}$. (d) Capillary-gravity-flexural wave at air-water interface with $\omega = 1.04 \times 10^3\,\mathrm{s}^{-1}$.

and has no displacement in that direction, so that the cross sections shown in Fig. 3 and Fig. 8 are independent of the y coordinate, which is perpendicular to the plotted xz plane. We include animated versions of all displacement plots in the Supplemental Material (SM) [61]. Comparing the Lucassen wave at the water-water interface in Fig. 3(a) to the capillary-gravity-flexural wave at the water-water interface in Fig. 3(c), the most prominent difference is that the displacement of the interface is purely longitudinal (in the x direction) for the Lucassen wave, while for the capillary-gravity-flexural wave, the displacement of the interface is purely transversal (in the z direction). Away from the interface, both Lucassen and capillary-gravity-flexural waves have finite longitudinal as well as transversal displacements.

In addition to the displacements plots, we show pressure maps and velocity fields of the example waves discussed above in Fig. 4. The pressure is calculated as a perturbation to the steady state solution of a fluid at rest and is given by [22]

$$P_M(\boldsymbol{r}, t) = P_0 - K_M \boldsymbol{\nabla} \cdot \boldsymbol{u}_M, \tag{48}$$

where P_0 is the pressure at $z = 0$. In our pressure maps, we show only the difference of pressure in the bulk to the pressure in the interface, i.e., we set $P_0 = 0$. Consistent with the surface-gravity approximation, we in Eq. (48) consider only the bulk pressure changes due to local compression
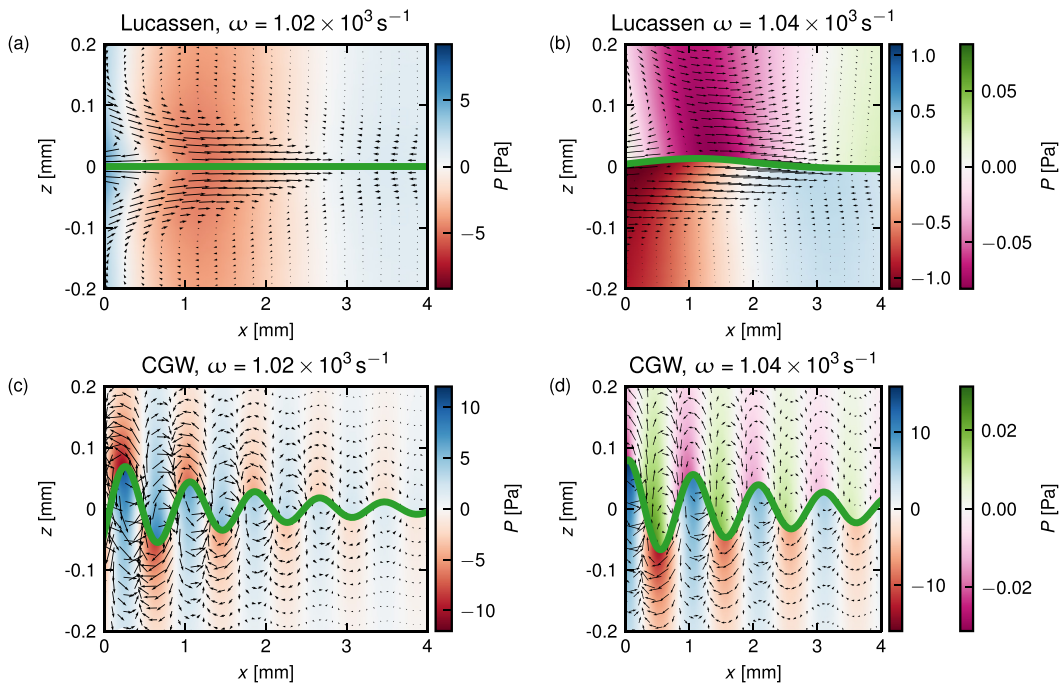
FIG. 4. Pressure maps and velocity fields corresponding to the waves shown in Fig. 3. Velocity fields are shown as black arrows, where arrow lengths correspond to the magnitude of the velocity. The pressure is shown as a heatmap, where a red-blue colormap is used for water pressure. The air pressure is indicated by a purple-green colormap. The pressure in the bulk fluids is always shown relative to the pressure at the interface, i.e., setting $P_0 = 0$ in Eq. (48). Scalings have been chosen equal to the plots shown in Fig. 3. (a) Lucassen wave at water-water interface with $\omega = 1.02 \times 10^3\,\mathrm{s}^{-1}$. (b) Lucassen wave at air-water interface with $\omega = 1.04 \times 10^3\,\mathrm{s}^{-1}$. (c) Capillary-gravity-flexural wave at water-water interface with $\omega = 1.02 \times 10^3\,\mathrm{s}^{-1}$. (d) Capillary-gravity-flexural wave at air-water interface with $\omega = 1.04 \times 10^3\,\mathrm{s}^{-1}$.

and expansion of the fluid. The velocity field is obtained by taking the temporal derivative of the harmonic wave ansatz (3). Pressures and velocity fields at frequencies higher than the first crossover frequency are shown in Fig. 9 in Appendix E. We include animated versions of all pressure plots in the SM [61]. Comparing the pressure profile of the Lucassen wave at the water-water interface in Fig. 4(a) to the pressure profile of the capillary-gravity-flexural wave at the water-water interface in Fig. 4(c), the most prominent difference is that the capillary-gravity-flexural wave has pressure nodes at the interface, i.e., changes in the sign of the pressure at the interface, whereas the Lucassen wave exhibits no pressure nodes. Instead it is very well seen that the Lucassen wave is a pressure wave along the interface. The velocity field for the Lucassen wave shows that velocities are predominantly directed towards and away from the direction of wave travel, and their magnitude decreases when moving away from the interface as well as from the site of initial excitation $x = 0$. For the capillary-gravity-flexural wave, the velocity field shows a rotating behavior, with the direction of rotation alternating from clockwise to counterclockwise at each pressure node. The decay lengths are comparable to those of the Lucassen wave.

3. Air-water interface

Experiments on lipid monolayers often measure membrane properties on a trough of water [8,13–15], which corresponds to a planar viscoelastic interface with water and air as bulk materials I and III. In theoretical modeling of air-water interfaces, one usually considers only the water dynamics

below the membrane, and does not explicitly consider the dynamics of the air above. This can be intuitively explained by the much lower density and viscosity of air in comparison to water. In this section, we compare predictions of our full dispersion relation (12) to the factorized half-space dispersion relation (35), to demonstrate that the air dynamics can indeed be neglected.

For medium I we use water, modeled as a compressible Newtonian fluid with the parameters from Sec. IV A 2. To model air as medium III, we also use the compressible Newtonian fluid model from Sec. IV A 1; at $25\,^{\circ}$C, the relevant parameters are [54] $\eta_{\text{III}} \approx 18.2 \times 10^{-6}\,\text{Pa s}$, $\eta'_{\text{III}} = 0$, $\rho_{\text{III}} \approx 1.2\,\text{kg/m}^3$, $c_{\text{III}} \approx 343\,\text{m/s}$.

For a wide range of frequencies, we numerically solve both the full dispersion relation (12) and the dispersion relations pertaining to each of the two factors of the half-space dispersion relation (35). We subsequently use Eqs. (15) and (16) to evaluate the corresponding phase velocities and propagation distances, and show the results in Figs. 2(b) and 2(d). For comparison, we also include the capillary-gravity-flexural wave solution of the full dispersion relation in the asymmetric case (32).

For the capillary-gravity-flexural wave, we observe that the phase velocities predicted by the full dispersion relation agree perfectly with the asymmetric dispersion relation throughout, and with the factorized half-space dispersion relation up until $\omega_{\text{I,d}} \equiv K_{\text{I}}/\eta'_{\text{I}} = 5 \times 10^{11}\,\text{s}^{-1}$; at this frequency, the dilational response of the water below the interface becomes dominated by the viscosity, and at $\omega_{\text{CG}}^{\max} = 3.41 \times 10^{11}\,\text{s}^{-1}$ the capillary-gravity-flexural wave solution disappears, similar to the symmetric case discussed in Sec. IV A 2 above. In contrast to the symmetric case, for the half-space, the phase velocity is not monotonic, but has a minimum at $\omega \approx 10^2\,\text{s}^{-1}$. This minimum denotes the crossover from capillarity-dominated to gravity-dominated dispersion, and its location follows from Eq. (44), by equating the left-hand side of the equation with the gravitational term, as

$$\omega_{\text{CG}} = \left(\frac{(\rho_{\text{I}} - \rho_{\text{III}})^3 g^3}{(\rho_{\text{I}} + \rho_{\text{III}})^2 \sigma_{\text{2D}}} \right)^{1/4} \approx 117\,\text{s}^{-1}, \tag{49}$$

where we use that for the frequencies and wave numbers involved $\tilde{\Pi}_{\text{2D}} \approx \sigma_{\text{2D}}$ holds, as follows from Eq. (14), and employ the gravity-wave dispersion relation (see just below) to eliminate k from the equation. For frequencies $\omega \ll \omega_{\text{CG}}$, the right-hand side of the dispersion relation (44) is dominated by the gravitational term, so that $k \approx \omega^2/g(\rho_{\text{I}} + \rho_{\text{III}})/(\rho_{\text{I}} - \rho_{\text{III}}) \sim \omega^2$. According to Eq. (18), we thus have $c \sim \omega^{-1}$, as observed in Fig. 2(b). This gravity-wave regime is not present in the symmetric scenario, because for $\rho_{\text{I}} = \rho_{\text{III}}$ the rightmost term in Eq. (44) vanishes. For the phase velocity of the Lucassen wave solution, we observe very good agreement between the full dispersion relation and the factorized half-space solution throughout. Even close to the frequency $\omega_{\text{CG}}^{\max} = 3.41 \times 10^{11}\,\text{s}^{-1}$, where the capillary-gravity-flexural wave solution disappears, the factorized Lucassen dispersion relation does not deviate from the full dispersion relation. This is in contrast to the symmetric scenario shown in Fig. 2(a), and presumably because, in the present case, $\omega_{\text{CG}}^{\max} = 3.41 \times 10^{11}\,\text{s}^{-1}$ is closer to the crossover frequency $\omega_{\text{2D}}^{\rho} = 10^{12}\,\text{s}^{-1}$, at which the inertia of the interface starts to dominate over bulk properties, so that the crossover in the bulk viscoelastic response is already less relevant for the dispersion relation.

The propagation distance of the capillary-gravity-flexural wave, shown in Fig. 2(d), displays a behavior similar to the symmetric case depicted in Fig. 2(c): For frequencies above $\omega_{\text{2D}}^{\sigma} \equiv \sigma_{\text{2D}}/\eta_{\text{2D}}^{\perp} = 5 \times 10^6\,\text{s}^{-1}$, where the surface viscosity dominates over the surface tension, the propagation distance of the full capillary-gravity-flexural wave agrees with the factorized half-space results. Below the crossover frequency $\omega_{\text{2D}}^{\sigma}$, the two formulas (12) and (35) predict different propagation distances. The propagation distance predicted by the full dispersion relation of the asymmetric case (32) agrees with the full dispersion relation even below $\omega_{\text{2D}}^{\sigma}$, except for very low frequencies $\omega \lesssim 10^2\,\text{s}^{-1}$. Also note that the propagation distances β^{-1} of the capillary-gravity-flexural wave scale differently than $\beta^{-1} \sim \omega^{-2}$, as observed in Fig. 2(d).

To summarize this section so far, for an air-water interface, the factorized half-space dispersion relation (35) overall constitutes a good approximation to the full dispersion relation (12) for both

capillary-gravity-flexural and Lucassen waves. However, for the capillary-gravity-flexural wave, the factorized equation fails to predict the breakdown of the wave at high frequencies, and overestimates the propagation distances at low frequencies.

As for the water-water case discussed above, we include example displacement plots of a Lucassen and capillary-gravity-flexural wave at $\omega \approx 10^3\,\mathrm{s}^{-1}$ in Figs. 3(b) and 3(d), respectively. Comparing the Lucassen wave at the air-water interface in Fig. 3(b) to the capillary-gravity-flexural waves at the air-water interface in Fig. 3(d), it transpires that the displacements in the Lucassen wave are dominated by longitudinal components, while the displacements of the capillary-gravity-flexural wave are dominated by transversal components. However, both the interface and the bulk fluids possess finite longitudinal and transversal components in both waves. For the Lucassen wave, there is an asymmetry in the vertical decay lengths: the vertical decay length of air $1/\mathrm{Re}(\lambda_{\mathrm{III,t}}^{-1})$ is significantly larger than its counterpart for water, $1/\mathrm{Re}(\lambda_{\mathrm{I,t}}^{-1})$. Meanwhile, for the capillary-gravity-flexural wave, the dominating vertical decay lengths $1/\mathrm{Re}(\lambda_{\mathrm{I,l}}^{-1})$ and $1/\mathrm{Re}(\lambda_{\mathrm{III,l}}^{-1})$ are symmetrical. As before, we additionally show pressure maps and velocity fields of the Lucassen and capillary-gravity-flexural waves at the air-water interface in Figs. 4(b) and 4(d). For the Lucassen wave, it transpires that both the air half-space and the water half-space exhibit regions of alternating negative and positive pressure, corresponding to the compression and expansion of the interface, similarly to the water-water case. However, the regions of maximum pressure in the two half-spaces do not perfectly align. For the capillary-gravity-flexural wave, as for the water-water interface shown in Fig. 4(c), there are pressure nodes visible, however they are slightly shifted along the x direction, meaning that absolute pressure maxima do not coincide for the two bulk fluids.

Comparing the Lucassen wave at the water-water interface in Fig. 3(a) to the Lucassen wave at the air-water interface in Fig. 3(b), the most prominent difference is that the motion of the water-water interface is purely longitudinal, while the motion of the air-water interface possesses also a transversal component. This is due to the asymmetry in the vertical decay lengths $1/\mathrm{Re}(\lambda_{\mathrm{I,t}}^{-1})$ and $1/\mathrm{Re}(\lambda_{\mathrm{III,t}}^{-1})$, respectively. Also note that the horizontal decay length $1/\mathrm{Im}(k)$ is larger in the asymmetric case than in the symmetric case. Comparing the capillary-gravity-flexural wave at the water-water interface in Fig. 3(c) to the capillary-gravity-flexural wave at the air-water interface in Fig. 3(d), the overall displacements look rather similar. The dominating vertical decay lengths are given by $1/\mathrm{Re}(\lambda_{\mathrm{I,l}}^{-1})$ and $1/\mathrm{Re}(\lambda_{\mathrm{III,l}}^{-1})$, which are equal in both the water-water and air-water scenario. As for the Lucassen wave, also for the capillary-gravity-flexural wave the horizontal decay length $1/\mathrm{Im}(k)$ is larger for the air-water case as compared to the water-water case. The motion of the water-water interface is purely transversal, while the air-water interface possesses a longitudinal component. To sum up, the displacement of the water-water interface is purely longitudinal for the Lucassen wave and purely transversal for the capillary-gravity-flexural wave, while differences in bulk fluids introduce an additional transversal and longitudinal component to the interface, respectively. Overall, horizontal decay lengths are larger in the air-water case than in the water-water case.

B. Viscoelastic bulk media

One advantage of both our general dispersion relation (12) and the factorized dispersion relation (21) is that these relations are derived for arbitrary linear, homogeneous, isotropic viscoelastic bulk media. While in the previous Sec. IV A we used Newtonian fluids as bulk media, in the present section we consider interfacial waves for two other viscoelastic bulk materials.

More explicitly, we consider the dispersion relation of the Lucassen wave solution on polymer gels and polymer solutions as bulk media. We here focus on the Lucassen wave, as this is the relevant pressure wave for biological scenarios related to nerve pulse propagation [15,16]. In particular, a viscoelastic membrane surrounded by two viscoelastic media serves as a model for the cell membrane of a neuron, separating the hydrogel axoplasm and extracellular fluid.

1. Polymer gels as bulk media: Kelvin-Voigt model

The elastic properties of polymer gels are determined by the density of entanglements between individual polymer chains. A characteristic of a gel are the extremely long lifetimes of entanglements. On timescales relevant to the wave phenomena we investigate, we can therefore assume permanent crosslinks between chains [62]. In the linear regime, the polymer gel can thus be modeled as a purely elastic polymer network immersed in a viscous Newtonian solvent. We model this as a Kelvin-Voigt material. For this, we leave the dilational relaxation function (41) unchanged, and use a shear relaxation function

$$\tilde{g}_{M,\text{s}}(\omega) = 2\eta_M + \frac{2E_M}{-i\omega}, \tag{50}$$

where η_M is the fluid viscosity, while E_M is the fluid elastic modulus under shear. A systematic bottom-up theory for the linear frequency-dependent viscoelastic response of a polymeric network can be found in Ref. [63]. On a phenomenological level, the Kelvin-Voigt model corresponds to a viscoelastic circuit comprised of a purely viscous damper and purely elastic spring, connected in parallel [41,42].

From Eq. (50) the characteristic crossover frequency of the Kelvin-Voigt material follows as

$$\omega_M^{\text{KV}} = \frac{E_M}{\eta_M}, \tag{51}$$

below which the shear response is dominated by elasticity, $\tilde{g}_{M,\text{s}}(\omega) \approx 2E_M/(-i\omega)$. Above the crossover frequency ω_M^{KV}, the shear response is approximately that of a Newtonian fluid, i.e., $\tilde{g}_{M,\text{s}}(\omega) \approx 2\eta_M$, which is constant as a function of ω. Equation (51) implies that the Kelvin-Voigt material has a characteristic timescale of $\tau_M^{\text{KV}} = 1/\omega_M^{\text{KV}}$.

Starting from the analytical solution of the generalized Lucassen wave (26) and inserting the shear relaxation function (50) for $\lambda_{M,\text{t}}$ in Eq. (9), we obtain the analytical Lucassen-wave solution for a viscoelastic membrane at the interface of two polymer gels as

$$k = \sqrt{\frac{\rho_{2\text{D}}\omega^2 + e^{i\pi/4}(\sqrt{R_\text{I}(\omega)} + \sqrt{R_\text{III}(\omega)})}{K_{2\text{D}} - i\omega\eta_{2\text{D}}}}, \tag{52}$$

where

$$R_M(\omega) = \rho_M\eta_M\omega^3\left(1 + i\frac{\omega_M^{\text{KV}}}{\omega}\right), \tag{53}$$

and where all complex square roots are chosen to have positive real part. For $\omega \gg \omega_M^{\text{KV}}$, we have $R_M(\omega) \approx \rho_M\eta_M\omega^3$ and Eq. (52) reduces to the Lucassen dispersion relation for a Newtonian fluid, Eq. (46).

As an explicit example we consider a symmetric system with Kelvin-Voigt bulk media, with elastic moduli $E \equiv E_\text{I} = E_\text{III} = 0.1\,\text{Pa}$, as in Ref. [62]. For the other bulk and interface parameters we use the same as in Sec. IV A 2; according to Eq. (51), this results in a Kelvin-Voigt crossover frequency $\omega^{\text{KV}} = 10^2\,\text{s}^{-1}$.

In Figs. 5(a) and 5(c), we compare the predictions of Eq. (52) to both the full symmetric dispersion relation (30), and the factorized Lucassen relation (46) for a symmetric Newtonian fluid system. As expected, for $\omega \gg \omega_M^{\text{KV}}$ the two factorized solutions (46) and (52) lead to indistinguishable phase velocities and propagation distances and differ only for $\omega \lesssim \omega_M^{\text{KV}}$, when the elastic component in Eq. (50) is nonnegligible. A solution that is similar to the Lucassen wave for the full dispersion relation (30) exists only in the frequency range $\omega > \omega_{\text{KV}}^{\min} = 2.29\,\text{s}^{-1}$, where it is well described by Eq. (52), except for a discontinuity at the frequency $\omega = 8.4 \times 10^{10}\,\text{s}^{-1}$, as observed in Sec. IV A 3. To rationalize the low-frequency breakdown of the Lucassen wave, we show in Appendix F that as ω approaches $\omega_{\text{KV}}^{\min} = 2.29\,\text{s}^{-1}$ from above, the real part of λ_t^{-1} approaches zero, so that the transversal
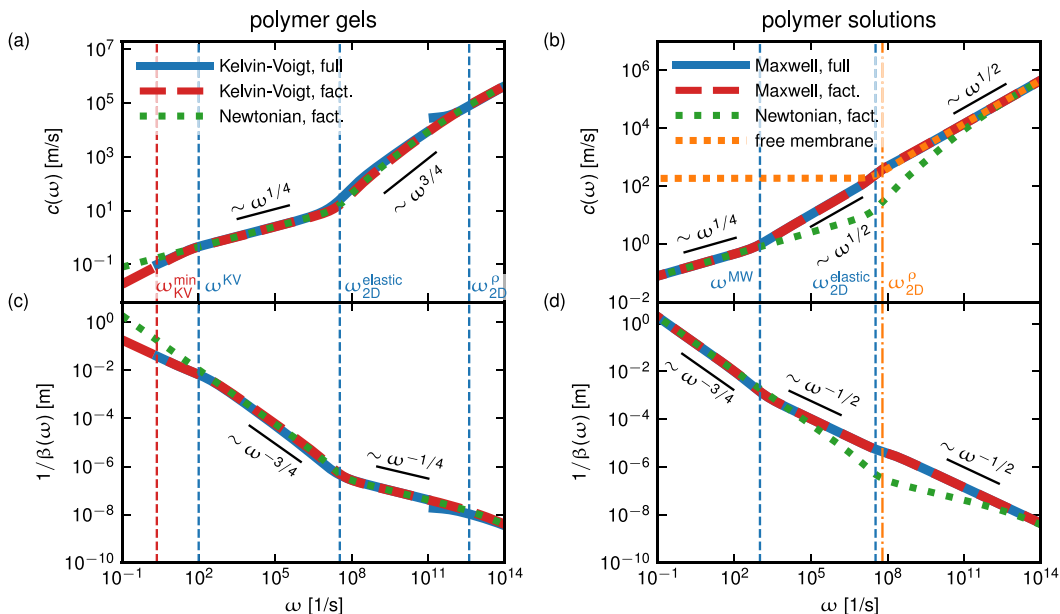
FIG. 5. Phase velocities c and propagation distances β^{-1} for Lucassen waves at an interface separating viscoelastic materials. Phase velocities and propagation distances are obtained from $k(\omega)$ via Eqs. (15) and (16). For (a) and (c), the viscoelastic bulk materials are two Kelvin-Voigt materials with identical properties, as discussed in Sec. IV B 1. To obtain $k(\omega)$, the full symmetric dispersion relation (30) (solid blue line), the Kelvin-Voigt Lucassen dispersion relation (52) (dashed red line), and the Newtonian-fluid Lucassen dispersion relation (46) (dotted green line) are evaluated numerically. For (b) and (d), two Maxwell fluids with identical parameters are considered as bulk materials; cf. Sec. IV B 2. To obtain $k(\omega)$, each of the dispersion relations (30) (solid blue line), (39) (dotted orange line), (46) (dotted green line), (55) (dashed red line) is evaluated numerically. For all subplots, vertical dashed lines denote crossover frequencies as discussed in Sec. IV B 1 for (a), (c), and in Sec. IV B 2 for (b), (d). Blue dashed lines denote crossovers in the Lucassen wave. Red dashed lines highlight the frequencies at which solutions of the full dispersion relation disappear. The crossover to the free membrane limit is colored orange for better distinguishability. The power-law scalings of c and β^{-1} within each scaling regime are indicated by black bars.

decay length of the Lucassen wave diverges. The wave solution therefore does not decay any longer away from the interface and hence ceases to be a surface wave solution.

In summary, we observe that the Lucassen wave breaks down for angular frequencies shortly below ω_{KV}^{min}, when the bulk media responds predominantly elastically. For angular frequencies above ω_{KV}^{min}, the Lucassen wave behaves as the corresponding wave solution for purely viscous fluids, as seen in Figs. 2(a) and 2(c), and in particular displays the same scaling regimes.

2. Polymer solutions as bulk media: Maxwell model

In contrast to the polymeric gel, the elastic properties of a solution of rather short polymer chains in liquid solvent are determined by finite lifetime interchain entanglements. Polymer chains may disentangle themselves from neighboring chains by diffusion, a process called reptation [62]. The characteristic time of a chain to diffuse out of the loose polymer network is called reptation time, and the characteristic macroscopic stress relaxation time $\tau_M \equiv 1/\omega_M^{MW}$ of such a polymer solution scales directly with the reptation time [62]. A polymer solution can be modeled as a Maxwell fluid

with shear relaxation function

$$\tilde{g}_{M,s}(\omega) = \frac{2\eta_M}{1 - i\omega\tau_M}, \tag{54}$$

which for small angular frequency $\omega \ll \omega_M^{MW} = 1/\tau_M$ reduces to the Newtonian fluid model (40). On a phenomenological level, a Maxwell fluid corresponds to a purely viscous damper and a purely elastic spring, connected in series [41,42]. This is in contrast to the Kelvin-Voigt model, where damper and spring are connected in parallel. While the Maxwell model describes a fluid, meaning that it features a purely viscous response in the low-frequency limit $\omega \ll \omega_M^{MW}$, the Kelvin-Voigt model describes a solid with a purely elastic response in the limit $\omega \ll \omega_M^{KV}$. It should be noted that real polymer gels are in fact described by more than two viscoelastic regimes and must be modeled by a combination of Kelvin-Voigt and Maxwell models.

The relevance of the Maxwell model goes beyond polymer solutions: As mentioned in Sec. IV A 2, in the THz regime also pure water deviates from a Newtonian fluid model, and descriptions of water on such short timescales are based on the Maxwell model and generalizations thereof [42]. For high-concentration glycerol solutions, non-Newtonian behavior in the shear viscosity can be observed at lower frequencies, namely in the GHz regime [42].

Substituting the Maxwell-model shear relaxation function into the generalized Lucassen wave (26), we obtain

$$k = \sqrt{\frac{\rho_{2D}\omega^2 + e^{i\pi/4}\left(\sqrt{\frac{\rho_I \eta_I \omega^3}{1 - i\omega\tau_I}} + \sqrt{\frac{\rho_{III}\eta_{III}\omega^3}{1 - i\omega\tau_{III}}}\right)}{K_{2D} - i\omega\eta_{2D}}}, \tag{55}$$

which for $\omega \ll \omega_M^{MW} \equiv 1/\tau_M$ reduces to the dispersion relation (46) of a Newtonian fluid.

As an example, we consider a symmetric system with Maxwell fluids as bulk media. For the characteristic Maxwell frequency we use $\omega^{MW} \equiv \omega_I^{MW} = \omega_{III}^{MW} = 10^3 \, \text{s}^{-1}$, so that $\tau \equiv 1/\omega^{MW} \equiv \tau_I = \tau_{III} = 10^{-3} \, \text{s}$. For all other bulk and interface parameters we consider the same values as in Sec. IV A 2.

In Figs. 5(b) and 5(d), we compare phase velocities and propagation distances based on Eq. (55) to those obtained from the full symmetric dispersion relation (30) and the Lucassen wave dispersion relation for a Newtonian fluid, Eq. (46). For frequencies $\omega \ll \omega^{MW}$, where the Maxwell fluid behaves like a Newtonian fluid, all three dispersion relations lead to identical phase velocities and propagation distances, with a scaling that follows from Eqs. (17) and (18), and the classical Lucassen wave scaling $k \sim \omega^{3/4}$, as previously observed in Figs. 2(a) and 2(c). This is in contrast to the Kelvin-Voigt model considered in the section above, where the solution differs from that of a Newtonian fluid for frequencies *below* the characteristic crossover frequency. For frequencies $\omega \gg \omega^{MW}$, the approximate scaling behavior of Eq. (55) can be obtained by considering the numerator and denominator inside the square root separately. We first consider the numerator. Using Eq. (28), and approximating $\tilde{g}_s \approx 2\eta/(-i\omega\tau)$ as appropriate for $\omega \gg \omega^{MW}$, the crossover from bulk-dominated to interface-dominated inertia occurs at the angular frequency $\omega_{2D}^\rho = 2\sqrt{\rho\eta/\tau}/\rho_{2D} \approx 6.3 \times 10^7 \, \text{s}^{-1}$; this crossover here occurs at a significantly lower frequency as compared to a Newtonian fluid with the same density and viscosity, for which in Sec. IV A 2 we obtained $10^{12} \, \text{s}^{-1}$. Interestingly, such a behavior is not seen in the Kelvin-Voigt model solution above. The crossover from elastic to viscous interface response, described by the denominator of the dispersion relation (55), follows via Eq. (29) as $\omega_{2D}^{elastic} = K_{2D}/\eta_{2D} = 3.4 \times 10^7 \, \text{s}^{-1}$, which for our system parameters is very close to ω_{2D}^ρ. For $\omega^{MW} \ll \omega \ll \omega_{2D}^{elastic}, \omega_{2D}^\rho$, the dispersion relation is dominated by bulk inertia and interface elasticity; the wave number scales approximately as $k \sim (\sqrt{\rho\eta/\tau}\omega/K_{2D})^{1/2} \sim \omega^{1/2}$, which according to Eq. (18) implies $c \sim \omega^{1/2}$, $\beta^{-1} \sim \omega^{-1/2}$. In this non-Newtonian frequency regime, the dispersion relations (55) and (30) agree perfectly, and are markedly different from the Newtonian fluid (46). This is in contrast to the Kelvin-Voigt model, where viscoelastic and Newtonian solutions coincide for frequencies *above* the characteristic crossover frequency. For $\omega \gg \omega_{2D}^{elastic}, \omega_{2D}^\rho$, the Lucassen wave is dominated by interfacial inertia and interface viscosity, and the wave number
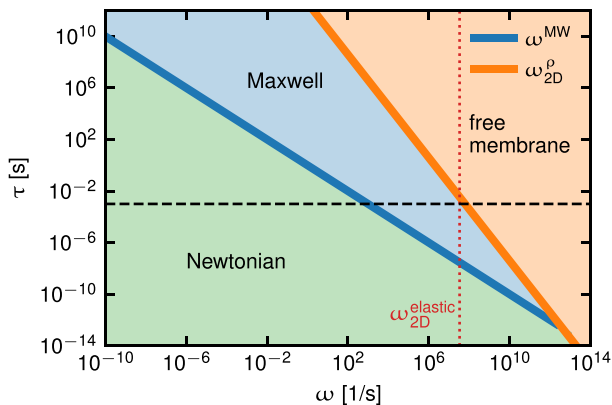
FIG. 6. Phase diagram showing the crossover frequencies found from the analytical solution of the Lucassen wave on the polymer solution-polymer solution interface Eq. (55). The crossover from Newtonian to Maxwell-fluid is denoted by ω^{MW} (blue line), whereas the crossover to the free membrane limit is denoted by ω_{2D}^{ρ} (orange line). The red dotted line shows the crossover from elastic to viscous response $\omega_{2D}^{elastic}$. The black dashed line shows our choice of $\tau = 10^{-3}$ s as an example.

scales as $k \sim \sqrt{\rho_{2D}\omega/\eta_{2D}} \sim \omega^{1/2}$, so that the scaling $c \sim \omega^{1/2}$, $\beta^{-1} \sim \omega^{-1/2}$ also holds at this frequency. That the dispersion relation is dominated by the interface for high frequencies is highlighted by the free-interface dispersion relation (39), which is also shown in Figs. 5(b) and 5(d), and which agrees with the Maxwell dispersion relations for $\omega \gg \omega_{2D}^{elastic}$, ω_{2D}^{ρ}. The interface dominance is also the reason why the Newtonian-fluid dispersion relation starts to agree with the Maxwell-fluid dispersion relation again at the highest frequencies shown: The bulk properties are simply not relevant anymore.

In Fig. 6 we show a phase diagram illustrating the crossover frequencies of the Lucassen wave solution for a viscoelastic membrane surrounded by two half-spaces consisting of a polymer solution in water, described by a Maxwell-fluid model, where we denote our choice of $\tau = 10^{-3}$ s with a black dashed line. It can be seen that for higher values of τ, the two crossovers happen at frequencies further away from each other, whereas for smaller values of τ, the crossover frequencies converge, until eventually the transition from the Newtonian-fluid behavior to the free membrane limit occurs without an intermediate Maxwell-model regime. The vertical red dotted line denotes the crossover frequency $\omega_{2D}^{elastic}$ from elastic to viscous interfacial response, as defined in Eq. (29). This line intersects the horizontal black dashed line very closely to the crossover from bulk-dominated Maxwell-model dispersion to free-membrane interface-dominated dispersion, highlighting again that the two crossovers (bulk to interface dominated wave; elastic to viscous interfacial response) occur simultaneously in Figs. 5(b) and 5(d).

In summary, we observe that the Lucassen wave at the interface of Maxwell fluids introduces two new scaling regimes with a power law $k \sim \omega^{1/2}$, which are distinctly different from the corresponding wave solution in the purely viscous case except for the highest frequencies shown. Moreover, the crossover frequency ω_{2D}^{ρ} marking the dominance of the interface properties over bulk properties occurs at a lower frequency than in the corresponding Newtonian-fluid case.

V. DISCUSSION AND CONCLUSIONS

In the present work we derive the general conditional equation (12), which governs linear waves at planar viscoelastic interfaces that separate two linear, homogeneous, isotropic viscoelastic bulk materials. We show how viscoelastic Rayleigh waves, and generalizations of capillary-gravity-flexural and Lucassen waves, as well the equations from elastic plate theory, follow from

our general relation. Focusing mainly on the Lucassen wave, we numerically solve the general dispersion relation, and compare the result to analytical limiting cases, for several explicit example systems, including a viscoelastic interface separating two Newtonian fluids, Kelvin-Voigt materials, and Maxwell fluids. For each case we identify and interpret the intermediate power-law scaling regimes of the wave phase velocity and propagation distance. Quantifying existence regimes and studying interrelations between different limiting cases is only possible via a theory which incorporates all relevant properties simultaneously. Our discussion of crossovers (Fig. 2 and Fig. 5) thus has to be based on such a unifying theory, which we provide in Sec. II.

From a theoretical perspective, our work unifies the derivation of a wide variety of surface waves, and uncovers relations between them. For example, our results make explicit that oscillations of an elastic plate in vacuum are in fact a limiting case of capillary-gravity-flexural waves. Our theory thus enables to systematically study the interrelations and parameter- and frequency-dependent crossovers between different wave solutions. This will in particular serve as a bridge to connect the extensive literature on waves on viscoelastic materials [64–66] to the literature on water wave theory [3,4,67].

From a more practical perspective, our results have several applications: Just as viscoelastic Rayleigh waves can be used to measure properties of the material they are excited on [38], or the damping of capillary waves can be used to infer the viscosity of a Newtonian fluid [68], the dispersion relations we derive here can be used to determine mechanical properties of both interface and bulk media, a topic which continues to be of importance in soft matter physics [38,56,69,70]. More explicitly, after experimentally identifying the various power-law scaling regimes of phase velocity and propagation distance of periodically excited Lucassen waves, the analytical viscoelastic Lucassen dispersion relation can be inverted to extract the characteristic viscoelastic timescales of the system under consideration. In particular, the high-frequency properties of viscoelastic surface waves provide a route to probe the non-Newtonian nature of water on short time scales; here, the surface-wave approach can complement established bulk-based experiments [52].

From a biophysical perspective, our theory for Lucassen waves in the presence of viscoelastic bulk media serves as a starting point for investigating the properties of interfacial sound pulses as carriers of information, which has possible relevance for acoustic nerve pulse propagation phenomena [13–15]. Interfaces in biological systems are typically immersed in a hydrogel environment, for which a viscoelastic description is more appropriate than a simple Newtonian fluid model. In this context it will be particularly interesting to understand how bulk viscoelasticity changes the properties of nonlinear sound waves at interfaces, which so far have exclusively been studied for Newtonian bulk fluids [15,16]. One particularly interesting aspect of the Lucassen wave is the dependence of phase velocities and propagation distances on the membrane compressibility K_{2D}, which according to Eqs. (15), (16), and (46), is, for a wave dominated by membrane elasticity and viscous bulk inertia, given by

$$c \sim \sqrt{K_{2D}}, \tag{56}$$

$$\beta^{-1} \sim \sqrt{K_{2D}}. \tag{57}$$

In our continuum model, modifications in the physical system under consideration are incorporated by changing the model parameters. For example, an axon membrane with a myelin sheath around it can be modeled as an effective interface, with an effective area modulus K_{2D}, assuming that myelin sheath and axon membrane are rigidly connected. Although direct experimental measurements are lacking, it is predicted that a myelin membrane has a larger area modulus K_{2D} as compared to the membrane of an unmyelinated axon [23,71–73]. We would therefore expect that myelination increases the area modulus of the effective axon interface, which according to Eqs. (56) and (57) would then both speed up pressure waves and enhance their propagation distance. As has been noted before in the context of pressure waves in cylinders [23], this acceleration of the pulse is similar to what is observed in saltatory conduction, where myelinated axons lead to action potentials that travel

TABLE I. Parameters appearing in our description of the viscoelastic media. For the bulk media parameters, the index $M \in \{$I, III$\}$ labels the medium.

Bulk media	
$\tilde{g}_{M,\mathrm{s}}(\omega)$	Shear relaxation function
$\tilde{g}_{M,\mathrm{d}}(\omega)$	Dilational relaxation function
ρ_M	(Volume) mass density
η_M	Shear viscosity
η'_M	Dilational viscosity
K_M	Bulk modulus
E_M	Elastic modulus in Kelvin-Voigt model
τ_M	Stress relaxation time in Maxwell model
c	Speed of sound
P	Pressure
Interface	
$\eta_{2\mathrm{D}}$	In-plane shear viscosity
$\eta'_{2\mathrm{D}}$	In-plane dilational viscosity
$\eta_{2\mathrm{D}}^{\perp}$	Transversal shear viscosity
$\kappa_{2\mathrm{D}}$	Bending rigidity
$-\sigma_{2\mathrm{D}}$	2D pressure
$\rho_{2\mathrm{D}}$	(Area) mass density
$\tilde{g}_{2\mathrm{D}}(\omega)$	In-plane relaxation function
$\tilde{\Pi}_{2\mathrm{D}}$	Out-of-plane relaxation function
Bulk media and interface	
g	Gravitational acceleration

faster, as compared to their unmyelinated counterparts. We emphasize that this is not the textbook view on saltatory conduction, for which compelling explanations already exist in the framework of the Hodgkin-Huxley model. Similarly, if anesthetics solvated in the lipid membrane indeed decrease the area modulus $K_{2\mathrm{D}}$, as suggested in Ref. [23], the Meyer-Overton rule, which states that the effectiveness of an anesthetic is directly proportional to its solubility in a lipid membrane [74,75], would be fully consistent with the properties of the Lucassen wave, which according to Eqs. (56) and (56) leads to slower and more strongly damped waves, and hence less efficient pulse propagation. Again, we stress that also for the Meyer-Overton phenomenon, there exist theories which do not utilize mechanical pulses as means of signal transduction [76–79].

A possible extension of this work includes the effects of a time-dependent external force acting on the interface, providing a theory to be used for surface microrheology [36,37]. Furthermore, it will be interesting to extend this work to other geometries, e.g., on cylinders, where one bulk fluid has finite depth and the interface is curved [80,81].

APPENDIX A: TABLE OF PARAMETERS

In Table I we summarize all parameters that appear in this paper. The parameters for media I, II, and III were all introduced in Sec. II.

APPENDIX B: DERIVATION OF HELMHOLTZ EQUATIONS

In the following we give a short derivation as to why potential functions $\tilde{\varphi}$ and $\tilde{\boldsymbol{\psi}}$ which solve the Helmholtz equations (4) and (5) also solve the linearized equations for momentum conservation (1) with viscoelastic stress-strain relation (2).

Since the convolutional integrals in Eq. (2) are considerably simpler in Fourier space, we start by writing the temporal Fourier transform of Eqs. (1) and (2) in the surface gravity approximation (cf. Ref. [22])

$$\rho_M(-i\omega)\tilde{u}_{M,j} = \partial_k\left(\tilde{g}_{M,\mathrm{s}}(\omega)\tilde{\epsilon}_{M,jk} + \frac{\delta_{ij}}{3}(\tilde{g}_{M,\mathrm{d}}(\omega) - \tilde{g}_{M,\mathrm{s}}(\omega))\tilde{\epsilon}_{M,ll}\right) \tag{B1}$$

for $j \in \{x, y, z\}$, where the components of the stress tensor are given by $\tilde{\epsilon}_{M,ij} = (\partial_j\tilde{u}_{M,k} + \partial_k\tilde{u}_{M,j})/2$ and the displacement is a function of space and frequency, $\tilde{\boldsymbol{u}}_M = \tilde{\boldsymbol{u}}_M(\boldsymbol{r}, \omega)$. We furthermore use the decomposition of the displacement into curl-free and divergence-free potentials (3), so that

$$\tilde{u}_{M,j} = \partial_j\tilde{\varphi}_M + \varepsilon_{jkl}\partial_k\tilde{\psi}_{M,l}, \tag{B2}$$

where ε_{jkl} denotes the three-dimensional Levi-Civita symbol [82]. We proceed to insert Eq. (B2) into Eq. (B1). A quick calculation yields that

$$\tilde{\epsilon}_{M,ll} = \mathrm{Tr}(\tilde{\boldsymbol{\epsilon}}_M) = \Delta\tilde{\varphi}_M, \tag{B3}$$

where $\Delta = \partial_x^2 + \partial_y^2 + \partial_z^2$ is the Laplace operator. After some mathematical transformations, we find furthermore that

$$\partial_k\tilde{\epsilon}_{M,jk} = \partial_j\Delta\tilde{\varphi}_M + \tfrac{1}{2}\varepsilon_{jkl}\partial_k\Delta\tilde{\psi}_{M,l}. \tag{B4}$$

Combining Eqs. (B2), (B3), and (B4) into Eq. (B1), one obtains

$$\rho_M(-i\omega)(\partial_j\tilde{\varphi}_M + \varepsilon_{jkl}\partial_k\tilde{\psi}_{M,l}) = \tilde{g}_{M,\mathrm{s}}\left(\partial_j\Delta\tilde{\varphi}_M + \frac{1}{2}\varepsilon_{jkl}\partial_k\Delta\tilde{\psi}_{M,l}\right) + \frac{1}{3}(\tilde{g}_{M,\mathrm{d}} - \tilde{g}_{M,\mathrm{s}})\partial_j\Delta\tilde{\varphi}_M, \tag{B5}$$

finally leading to

$$0 = \partial_j\left(\rho_M(-i\omega)\tilde{\varphi}_M - \frac{1}{3}(2\tilde{g}_{M,\mathrm{s}} + \tilde{g}_{M,\mathrm{d}})\Delta\tilde{\varphi}_M\right) + \varepsilon_{jkl}\partial_k\left(\rho_M(-i\omega)\tilde{\psi}_{M,l} - \frac{1}{2}\tilde{g}_{M,\mathrm{s}}\Delta\tilde{\psi}_{M,l}\right). \tag{B6}$$

From the form of Eq. (B6) we can immediately see that if Eqs. (4) and (5) hold, then Eq. (B6) is fulfilled.

APPENDIX C: DERIVATION OF LINEAR SYSTEM OF EQUATIONS DETERMINING THE FULL DISPERSION RELATION

A review of the derivation of the continuum mechanical boundary conditions of two bulk media divided by a viscoelastic surface was given by Kralchevsky *et al.* [43]. The interface is assumed to have a purely viscous shear response with viscosity $\eta_{2\mathrm{D}}$, a viscoelastic response under dilation with viscosity $\eta'_{2\mathrm{D}}$ and a position-dependent surface tension σ. For out-of-plane deformations, a bending rigidity $\kappa_{2\mathrm{D}}$ and a transverse viscosity $\eta_{2\mathrm{D}}^{\perp}$ is taken into account. Furthermore, the interface has an area mass density $\rho_{2\mathrm{D}}$. In Ref. [22], it is shown that the surface tension of the interface can be written as

$$\sigma_{2\mathrm{D}}(\boldsymbol{r}, t) = \sigma_{2\mathrm{D}} + K_{2\mathrm{D}}\partial_\beta u_\beta, \tag{C1}$$
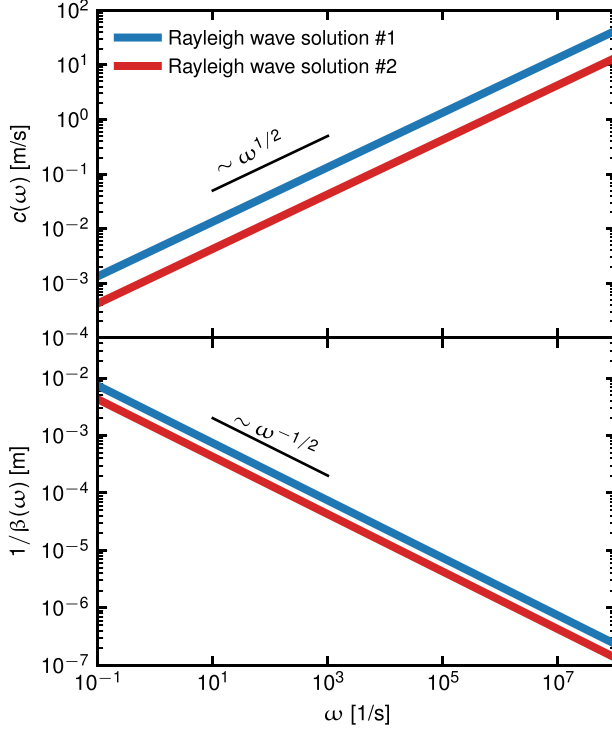
FIG. 7. Traditional Rayleigh wave solutions at the vacuum-water interface. The dispersion relation for the traditional Rayleigh wave equation (34) is solved numerically to obtain the wave number k as a function of ω. Phase velocities and propagation distances are obtained from $k(\omega)$ via Eqs. (15) and (16).

where σ_{2D} is the constant equilibrium surface tension, K_{2D} is the 2D modulus of compression of the surface, and we use the convention that Greek indices run over $\{x, y\}$, while Latin indices run over $\{x, y, z\}$. The position-dependent surface tension Eq. (C1) is necessary to model interfaces with insoluble surfactants, such as DPPC membranes on water. This is because insoluble surfactants do not simply move into the bulk upon compression of the membrane, which leads to a finite interfacial compressibility. In fact, only for a finite interfacial compressibility K_{2D} can interfacial pressure wave (Lucassen wave) solutions arise from the general dispersion relation, as is shown in Refs. [16,22]. Combining Eq. (C1) with the results of Ref. [43], the boundary conditions

$$\rho_{2D}\partial_t^2 u_{2D,\alpha} = (\sigma_{\text{III},z\alpha} - \sigma_{\text{I},z\alpha}) + (K_{2D} + \eta'_{2D}\partial_t)\partial_\alpha\partial_\beta u_{2D,\beta} + \eta_{2D}\partial_t\partial_\beta^2 u_{2D,\alpha}, \quad \text{for } \alpha \in \{x, y\}, \quad \text{(C2)}$$

$$\rho_{2D}\partial_t^2 u_{2D,z} = (\sigma_{\text{III},zz} - \sigma_{\text{I},zz}) - \rho_{2D}g(1 - \partial_\beta u_{2D,\beta}) + \left(\sigma_{2D} + \eta_{2D}^\perp\partial_t - \kappa_{2D}\partial_\beta^2\right)\partial_\beta^2 u_{2D,z} \quad \text{(C3)}$$

are derived in Ref. [22]. Here ρ_{2D} is the constant equilibrium surface excess mass area density of the interface, $\boldsymbol{u}_{2D}$ is the displacement of the interface, and all functions of position are understood to be evaluated at $z = 0$.

Including gravitational restoring forces in the boundary condition, the temporal Fourier transform of the stress tensor (2) at the interface $z = 0$ is given by [22]

$$\tilde{\sigma}_{jk}(\omega) = -\delta_{jk}[\delta(\omega)P_0 - g\rho\tilde{u}_z(\omega)] + (-i\omega)\tilde{g}_s(\omega)\tilde{\epsilon}_{jk}(\omega) + \delta_{jk}\frac{-i\omega}{3}[\tilde{g}_d(\omega) - \tilde{g}_s(\omega)]\tilde{\epsilon}_{ll}(\omega), \quad \text{(C4)}$$

where P_0 is the constant background pressure at $z = 0$ and the displacement field $\boldsymbol{u}$ and its derivatives are understood to be evaluated at $z = 0$. Note that according to the surface gravity

approximation [45], the gravitational acceleration of the bulk media only enters in the boundary conditions via Eq. (C4) [22].

The continuity conditions at the interface $z = 0$ are obtained by calculating the displacement field (3) from the harmonic wave ansatz (6) and (7) for $z > 0$ and $z < 0$, respectively, and equating them at $z = 0$. This yields the two linear equations

$$\begin{pmatrix} ik & -\lambda_{\mathrm{I,t}}^{-1} & -ik & -\lambda_{\mathrm{III,t}}^{-1} \\ \lambda_{\mathrm{I,l}}^{-1} & ik & \lambda_{\mathrm{III,l}}^{-1} & -ik \end{pmatrix} \begin{pmatrix} \Phi_{\mathrm{I}} \\ \Psi_{\mathrm{I}} \\ \Phi_{\mathrm{III}} \\ \Psi_{\mathrm{III}} \end{pmatrix} = \begin{pmatrix} 0 \\ 0 \end{pmatrix}, \tag{C5}$$

where $\lambda_{\mathrm{I,l}}^{-1}$, $\lambda_{\mathrm{I,t}}^{-1}$, $\lambda_{\mathrm{III,l}}^{-1}$, $\lambda_{\mathrm{III,t}}^{-1}$ are given by Eqs. (8) and (9). The stress continuity equations are obtained by calculating $\tilde{\sigma}_{\mathrm{I},ij}$, $\tilde{\sigma}_{\mathrm{III},ij}$ and $\tilde{u}_{\mathrm{2D},i} = (\tilde{u}_{\mathrm{I},i}|_{z=0} + \tilde{u}_{\mathrm{III},i}|_{z=0})/2$ for the displacement field (3), and then substituting the result into Eqs. (C2) and (C3). For Eq. (C2), only the $\alpha = x$ case is needed, since a short calculation shows that the $\alpha = y$ equation is fulfilled trivially. For the stress tensors of media I and III we use the generalized form (C4) to include effects of gravity [22]. The resulting equations for the stress boundary conditions are

$$\begin{aligned} 0 = {} & ik\big[i\omega\rho_{\mathrm{2D}} - k^2\tilde{g}_{\mathrm{2D}} - 2\tilde{g}_{\mathrm{I,s}}\lambda_{\mathrm{I,l}}^{-1}\big]\Phi_{\mathrm{I}} + \big[\lambda_{\mathrm{I,t}}^{-1}(-i\omega\rho_{\mathrm{2D}} + k^2\tilde{g}_{\mathrm{2D}}) + \tilde{g}_{\mathrm{I,s}}\big(k^2 + \lambda_{\mathrm{I,t}}^{-2}\big)\big]\Psi_{\mathrm{I}} \\ & + ik\big[i\omega\rho_{\mathrm{2D}} - k^2\tilde{g}_{\mathrm{2D}} - 2\tilde{g}_{\mathrm{III,s}}\lambda_{\mathrm{III,l}}^{-1}\big]\Phi_{\mathrm{III}} \\ & + \big[-\lambda_{\mathrm{III,t}}^{-1}(-i\omega\rho_{\mathrm{2D}} + k^2\tilde{g}_{\mathrm{2D}}) - \tilde{g}_{\mathrm{III,s}}\big(k^2 + \lambda_{\mathrm{III,t}}^{-2}\big)\big]\Psi_{\mathrm{III}} \end{aligned} \tag{C6}$$

and

$$\begin{aligned} 0 = {} & \big[\lambda_{\mathrm{I,l}}^{-1}(\omega^2\rho_{\mathrm{2D}} - k^2\tilde{\Pi}_{\mathrm{2D}} - 2g\rho_{\mathrm{I}}) - k^2\rho_{\mathrm{2D}}g + i\omega\tilde{g}_{\mathrm{I,s}}\big(k^2 + \lambda_{\mathrm{I,t}}^{-2}\big)\big]\Phi_{\mathrm{I}} \\ & + ik\big[\omega^2\rho_{\mathrm{2D}} - k^2\tilde{\Pi}_{\mathrm{2D}} - 2g\rho_{\mathrm{I}} + \lambda_{\mathrm{I,t}}^{-1}(2i\omega\tilde{g}_{\mathrm{I,s}} - g\rho_{\mathrm{2D}})\big]\Psi_{\mathrm{I}} \\ & + \big[-\lambda_{\mathrm{III,l}}^{-1}(\omega^2\rho_{\mathrm{2D}} - k^2\tilde{\Pi}_{\mathrm{2D}} + 2g\rho_{\mathrm{III}}) - k^2\rho_{\mathrm{2D}}g - i\omega\tilde{g}_{\mathrm{III,s}}\big(k^2 + \lambda_{\mathrm{III,t}}^{-2}\big)\big]\Phi_{\mathrm{III}} \\ & + ik\big[\omega^2\rho_{\mathrm{2D}} - k^2\tilde{\Pi}_{\mathrm{2D}} + 2g\rho_{\mathrm{III}} + \lambda_{\mathrm{III,t}}^{-1}(2i\omega\tilde{g}_{\mathrm{III,s}} + g\rho_{\mathrm{2D}})\big]\Psi_{\mathrm{III}}, \end{aligned} \tag{C7}$$

where again $\lambda_{\mathrm{I,l}}^{-1}$, $\lambda_{\mathrm{I,t}}^{-1}$, $\lambda_{\mathrm{III,l}}^{-1}$ and $\lambda_{\mathrm{III,t}}^{-1}$ are given by Eqs. (8) and (9), and where $\tilde{g}_{\mathrm{2D}}(\omega)$, $\tilde{\Pi}_{\mathrm{2D}}(k, \omega)$ are defined via Eqs. (13) and (14).

The homogeneous linear system of Eqs. (C5), (C6), and (C7) for the coefficients Φ_{I}, Ψ_{I}, Φ_{III} and Ψ_{III} has a nontrivial solution if and only if the determinant of the coefficient matrix is zero. Calculating this determinant and equating it with zero, we obtain the conditional Eq. (12).

APPENDIX D: RAYLEIGH WAVES AT THE VACUUM-FLUID INTERFACE

As discussed in Sec. III B, we find a Rayleigh-type surface wave equation for the water-vacuum interface. More explicitly, upon removing the effects related to the surface ($\rho_{\mathrm{2D}} = 0$, $\tilde{g}_{\mathrm{2D}} = 0$, $\tilde{\Pi}_{\mathrm{2D}} = 0$), Eq. (32) becomes Eq. (34):

$$4k^2\lambda_{\mathrm{I,l}}^{-1}\lambda_{\mathrm{I,t}}^{-1} = \big(k^2 + \lambda_{\mathrm{I,t}}^{-2}\big)^2.$$

This equation gives rise to two Rayleigh-type wave solutions $k(\omega)$. A plot showing the two solutions of Eq. (34) at the vacuum-water interface is shown in Fig. 7.

APPENDIX E: EXAMPLE VISUALIZATIONS IN THE DISSIPATIVE REGIME

We include example displacement plots of a Lucassen and capillary-gravity-flexural wave (CGW) at $\omega \approx 10^8\,\mathrm{s}^{-1}$ at the water-water interface in Figs. 8(a) and 8(c) and at the air-water interface in Figs. 8(b) and 8(d), respectively. As opposed to the plots in Fig. 3, all displacement fields are shown for frequencies above the first crossovers, i.e., in the dissipative regime. In this regime,
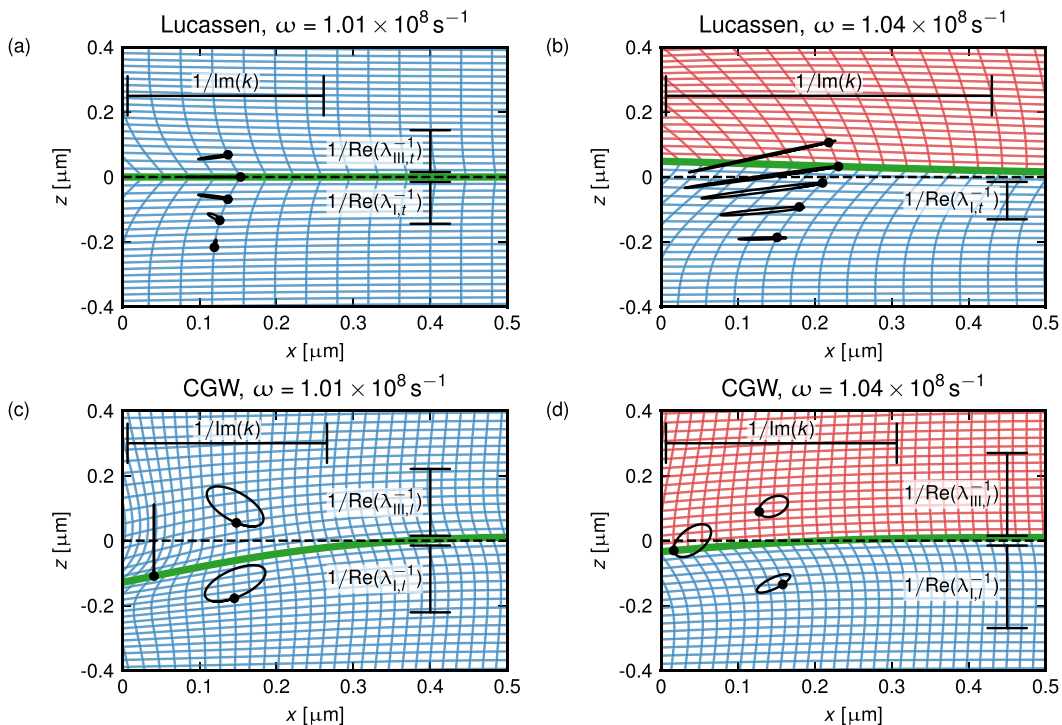
FIG. 8. Displacement plots of Lucassen and capillary-gravity-flexural waves (CGW) in the dissipative regime. The scaling is chosen such that the wave-type-specific dominant decay lengths into the bulk media $1/\mathrm{Re}(\lambda_{M,\mathrm{t}}^{-1})$ and $1/\mathrm{Re}(\lambda_{M,\mathrm{l}}^{-1})$ as well as the propagation distance $\beta^{-1} = 1/\mathrm{Im}(k)$ are of the same order of magnitude and visible in the plot. The displacement of the interface is shown as a green line. Bulk water displacement is shown as a blue grid, whereas bulk air displacement is shown as a red grid. Decay length and volume element trajectories are shown in black. (a) Lucassen wave at water-water interface with $\omega = 1.01 \times 10^8 \, \mathrm{s}^{-1}$. (b) Lucassen wave at air-water interface with $\omega = 1.04 \times 10^8 \, \mathrm{s}^{-1}$. Note that the vertical decay length into air $1/\mathrm{Re}(\lambda_{\mathrm{I,t}}^{-1})$ is too large to include in the diagram without rendering the displacements too small to observe. (c) Capillary-gravity-flexural wave at water-water interface with $\omega = 1.01 \times 10^8 \, \mathrm{s}^{-1}$. (d) Capillary-gravity-flexural wave at air-water interface with $\omega = 1.04 \times 10^8 \, \mathrm{s}^{-1}$.

the membrane response is dominated by the interfacial shear viscosity $\eta_{2\mathrm{D}}$ for the Lucassen wave and by the interfacial transversal viscosity $\eta_{2\mathrm{D}}^{\perp}$ for the capillary-gravity-flexural wave, respectively. Again, the water-water interface displacements are purely longitudinal for the Lucassen wave and purely transversal for the capillary-gravity-flexural wave, while the bulk fluid elements have finite longitudinal and transversal components in both cases.

In addition to the displacement plots, we include pressure maps and velocity fields of the example waves in the dissipative regime described above in Fig. 9. We include animated versions of all plots in the SM.

APPENDIX F: BREAKDOWN OF LUCASSEN WAVE ON KELVIN-VOIGT INTERFACE

As discussed in Sec. IV B 1, at $\omega_{\mathrm{KV}}^{\min} = 2.29 \, \mathrm{s}^{-1}$, the numerical Lucassen wave solution of Eq. (30) ceases to exist. In Fig. 10 we show that the real part of $\lambda_{\mathrm{t}}^{-1}(k, \omega)$ approaches zero as ω approaches $\omega_{\mathrm{KV}}^{\min} = 2.29 \, \mathrm{s}^{-1}$, so that the transversal decay length diverges; the wave hence ceases to be a surface wave, which rationalizes the breakdown of the Lucassen wave.
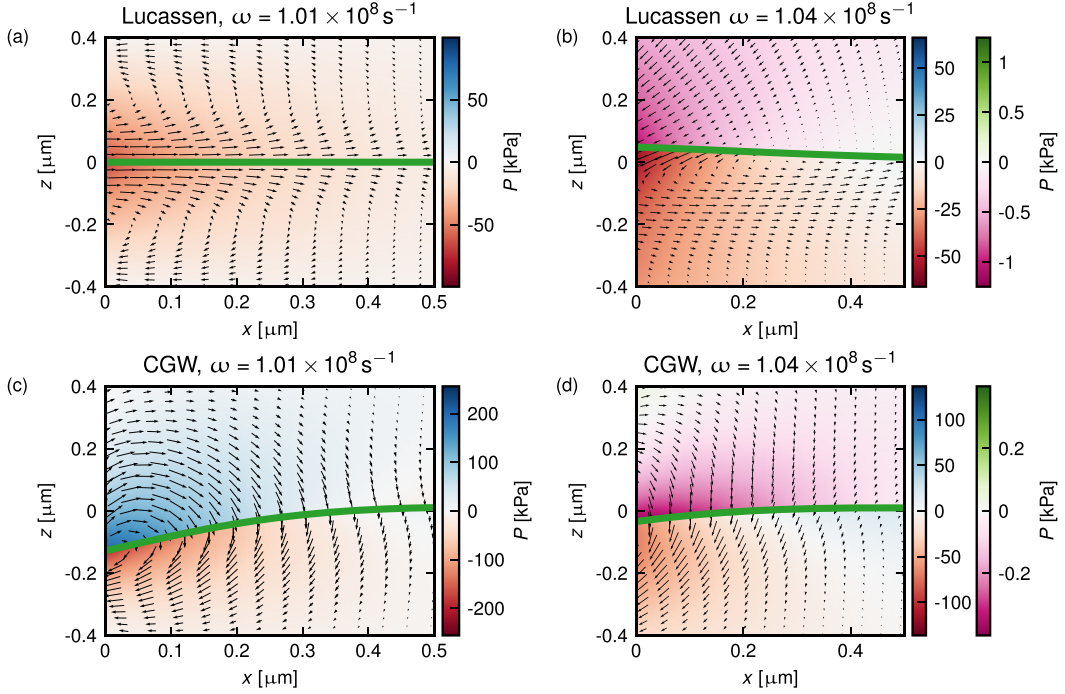
FIG. 9. Pressure maps and velocity fields corresponding to the waves shown in Fig. 8. Velocity fields are shown as black arrows, where arrow lengths correspond to the magnitude of the velocity. The pressure is shown as a heatmap, where a red-blue colormap is used for water pressure. The air pressure is indicated by a purple-green colormap. The pressure in the bulk fluids is always meant to be the difference to the pressure at the interface, i.e., $P_0 = 0$ in Eq. (48). Scalings have been chosen equal to the plots shown in Fig. 8. (a) Lucassen wave at water-water interface with $\omega = 1.01 \times 10^8 \, \text{s}^{-1}$. (b) Lucassen wave at air-water interface with $\omega = 1.04 \times 10^8 \, \text{s}^{-1}$. (c) Capillary-gravity-flexural wave at water-water interface with $\omega = 1.01 \times 10^8 \, \text{s}^{-1}$. (d) Capillary-gravity-flexural wave at air-water interface with $\omega = 1.04 \times 10^8 \, \text{s}^{-1}$.
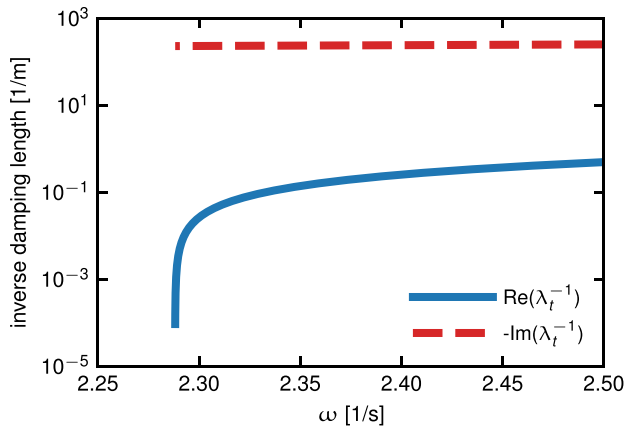

FIG. 10. Plot of real and imaginary parts of the inverse transversal damping length $\lambda_t^{-1}(k, \omega)$ in the frequency region of the breakdown of the Lucassen wave for a purely elastic membrane bounded by half-spaces of polymer gels modelled as Kelvin-Voigt fluids, obtained by inserting the numerical solution $k(\omega)$ of Eq. (30) into Eq. (9). Dashed lines show negative values.

[1] G. B. Airy, Tides and waves, in *Encyclopaedia Metropolitana*, Vol. 5, edited by H. J. Rose *et al.* (London, 1845).

[2] W. Thomson, Ripples and waves, Nature (London) **5**, 1 (1871).

[3] D. J. Acheson, *Elementary Fluid Dynamics*, Oxford Applied Mathematics and Computing Science Series (Clarendon, Oxford, 1990).

[4] L. D. Landau, E. M. Lifshitz, J. B. Sykes, and W. H. Reid, *Fluid Mechanics*, 2nd ed. (Pergamon Press, Oxford, 1987).

[5] A. D. D. Craik, The origins of water wave theory, Annu. Rev. Fluid Mech. **36**, 1 (2004).

[6] A. D. D. Craik, George Gabriel Stokes on water wave theory, Annu. Rev. Fluid Mech. **37**, 23 (2005).

[7] T. Chou, Band structure of surface flexural-gravity waves along periodic interfaces, J. Fluid Mech. **369**, 333 (1998).

[8] F. Monroy and D. Langevin, Direct Experimental Observation of the Crossover from Capillary to Elastic Surface Waves on Soft Gels, Phys. Rev. Lett. **81**, 3167 (1998).

[9] M. Van Den Tempel and R. P. Van De Riet, Damping of waves by surface-active materials, J. Chem. Phys. **42**, 2769 (1965).

[10] J. Lucassen, Longitudinal capillary waves. Part 1. Theory, Trans. Faraday Soc. **64**, 2221 (1968).

[11] J. Lucassen, Longitudinal capillary waves. Part 2. Experiments, Trans. Faraday Soc. **64**, 2230 (1968).

[12] J. Lucassen and M. Van Den Tempel, Longitudinal waves on visco-elastic surfaces, J. Colloid Interface Sci. **41**, 491 (1972).

[13] J. Griesbauer, A. Wixforth, and M. F. Schneider, Wave propagation in lipid monolayers, Biophys. J. **97**, 2710 (2009).

[14] J. Griesbauer, S. Bössinger, A. Wixforth, and M. F. Schneider, Propagation of 2D Pressure Pulses in Lipid Monolayers and Its Possible Implications for Biology, Phys. Rev. Lett. **108**, 198103 (2012).

[15] S. Shrivastava and M. F. Schneider, Evidence for two-dimensional solitary sound waves in a lipid controlled interface and its implications for biological signalling, J. R. Soc. Interface **11**, 20140098 (2014).

[16] J. Kappler, S. Shrivastava, M. F. Schneider, and R. R. Netz, Nonlinear fractional waves at elastic interfaces, Phys. Rev. Fluids **2**, 114804 (2017).

[17] Lord Rayleigh, On waves propagated along the plane surface of an elastic solid, Proc. London Math. Soc. **s1–17**, 4 (1885).

[18] P. K. Currie, M. A. Hayes, and P. M. Oleary, Viscoelastic Rayleigh-waves, Q. Appl. Math. **35**, 35 (1977).

[19] P. K. Currie and P. M. Oleary, Viscoelastic Rayleigh-waves II, Q. Appl. Math. **35**, 445 (1978).

[20] W. Lowrie, *Fundamentals of Geophysics*, 2nd ed. (Cambridge University Press, Cambridge, 2007).

[21] G. Hévin, O. Abraham, H. A. Pedersen, and M. Campillo, Characterization of surface cracks with Rayleigh waves: A numerical model, NDT & E Int. **31**, 289 (1998).

[22] J. Kappler and R. R. Netz, Multiple surface wave solutions on linear viscoelastic media, Europhys. Lett. **112**, 19002 (2015).

[23] M. M. Rvachev, On axoplasmic pressure waves and their possible role in nerve impulse propagation, Biophys. Rev. Lett. **05**, 73 (2010).

[24] B. Drukarch, H. A. Holland, M. Velichkov, J. J. G. Geurts, P. Voorn, G. Glas, and H. W. de Regt, Thinking about the nerve impulse: A critical analysis of the electricity-centered conception of nerve excitability, Prog. Neurobiol. **169**, 172 (2018).

[25] J. Engelbrecht, T. Peets, and K. Tamm, Electromechanical coupling of waves in nerve fibres, Biomech. Model. Mechanobiol. **17**, 1771 (2018).

[26] G. Fongang Achu, F. M. Moukam Kakmeni, and A. M. Dikande, Breathing pulses in the damped-soliton model for nerves, Phys. Rev. E **97**, 012211 (2018).

[27] L. Holland, H. W. de Regt, and B. Drukarch, Thinking about the nerve impulse: The prospects for the development of a comprehensive account of nerve impulse propagation, Front. Cell. Neurosci. **13**, 208 (2019).

[28] H. Barz, A. Schreiber, and U. Barz, Nerve impulse propagation: Mechanical wave model and HH model, Med. Hypoth. **137**, 109540 (2020).

[29] M. Mussel and M. F. Schneider, Sound pulses in lipid membranes and their potential function in biology, Prog. Biophys. Mol. Biol. **162**, 101 (2021).

[30] G. H. Kim, P. Kosterin, A. L. Obaid, and B. M. Salzberg, A mechanical spike accompanies the action potential in mammalian nerve terminals, Biophys. J. **92**, 3122 (2007).

[31] A. El Hady and B. B. Machta, Mechanical surface waves accompany action potential propagation, Nat. Commun. **6**, 6697 (2015).

[32] J. L. Harden and H. Pleiner, Hydrodynamic modes of viscoelastic polymer films, Phys. Rev. E **49**, 1411 (1994).

[33] A. J. Levine and F. C. MacKintosh, Dynamics of viscoelastic membranes, Phys. Rev. E **66**, 061606 (2002).

[34] G. K. Rajan and D. M. Henderson, Linear waves at a surfactant-contaminated interface separating two fluids: Dispersion and dissipation of capillary-gravity waves, Phys. Fluids **30**, 072104 (2018).

[35] G. K. Rajan, Dissipation of interfacial Marangoni waves and their resonance with capillary-gravity waves, Int. J. Eng. Sci. **154**, 103340 (2020).

[36] Y. Onodera and P.-K. Choi, Surface-wave modes on soft gels, J. Acoust. Soc. Am. **104**, 3358 (1998).

[37] C. Bar-Haim and H. Diamant, Surface response of a polymer network: Semi-infinite network, Langmuir **36**, 3981 (2020).

[38] X. Shao, J. R. Saylor, and J. B. Bostwick, Extracting the surface tension of soft gels from elastocapillary wave behavior, Soft Matter **14**, 7347 (2018).

[39] P. Chantelot, L. Domino, and A. Eddi, How capillarity affects the propagation of elastic waves in soft gels, Phys. Rev. E **101**, 032609 (2020).

[40] L. D. Landau, E. M. Lifshitz, A. M. Kosevich, and L. P. Pitaevskî, *Theory of Elasticity*, 3rd ed., Course of Theoretical Physics (Butterworth-Heinemann, Oxford, 1986).

[41] R. M. Christensen, *Theory of Viscoelasticity*, 2nd ed. (Academic Press, New York, 1982).

[42] J. C. F. Schulz, A. Schlaich, M. Heyden, R. R. Netz, and J. Kappler, Molecular interpretation of the non-Newtonian viscoelastic behavior of liquid water at high frequencies, Phys. Rev. Fluids **5**, 103301 (2020).

[43] P. A. Kralchevsky, J. C. Eriksson, and S. Ljunggren, Theory of curved interfaces and membranes: Mechanical and thermodynamical approaches, Adv. Colloid Interface Sci. **48**, 19 (1994).

[44] D. H. Everett, Manual of symbols and terminology for physicochemical quantities and units, Appendix II: Definitions, terminology and symbols in colloid and surface chemistry, Pure Appl. Chem. **31**, 577 (1972).

[45] P. Segall, *Earthquake and Volcano Deformation* (Princeton University Press, Princeton, 2010).

[46] If either λ_l^{-2} or λ_t^{-2} is purely real and negative, both square roots have vanishing real part, but we do not accept such solutions: The wave would not be damped away from the interface.

[47] E. H. Lucassen-Reynders and J. Lucassen, Properties of capillary waves, Adv. Colloid Interface Sci. **2**, 347 (1970).

[48] J. C. Earnshaw and E. McCoo, Mode Mixing of Liquid Surface Waves, Phys. Rev. Lett. **72**, 84 (1994).

[49] A. Mielke, R. R. Netz, and S. Zendehroud, A rigorous derivation and energetics of a wave equation with fractional damping, J. Evol. Eq. **21**, 3079 (2021).

[50] Sir H. Lamb, *Hydrodynamics*, 6th ed. (Cambridge University Press, Cambridge, 1975).

[51] I. Omelyan, I. Mryglod, and M. Tokarchuk, Wavevector- and frequency-dependent shear viscosity of water: The modified collective mode approach and molecular dynamics calculations, Condens. Matter Phys. **8**, 25 (2005).

[52] M. Pelton, D. Chakraborty, E. Malachosky, P. Guyot-Sionnest, and J. E. Sader, Viscoelastic Flows in Simple Liquids Generated by Vibrating Nanostructures, Phys. Rev. Lett. **111**, 244502 (2013).

[53] T. J. O'Sullivan, S. K. Kannam, D. Chakraborty, B. D. Todd, and J. E. Sader, Viscoelasticity of liquid water investigated using molecular dynamics simulations, Phys. Rev. Fluids **4**, 123302 (2019).

[54] R. E. Bolz and G. L. Tuve, *CRC Handbook of Tables for Applied Engineering Science*, 2nd ed. (CRC Press, 2019).

[55] J. Krögel, J. B. Li, R. Miller, M. Bree, G. Kretzschmar, and H. Möhwald, Surface viscoelasticity of phospholipid monolayers at the air/water interface, Colloid Polym. Sci. **274**, 1183 (1996).

[56] E. P. Petrov, R. Petrosyan, and P. Schwille, Translational and rotational diffusion of micrometer-sized solid domains in lipid membranes, Soft Matter **8**, 7552 (2012).

[57] E. P. Petrov and P. Schwille, Translational diffusion in lipid membranes beyond the Saffman-Delbrück approximation, Biophys. J. **94**, L41 (2008).

[58] C.-H. Lee, W.-C. Lin, and J. Wang, All-optical measurements of the bending rigidity of lipid-vesicle membranes across structural phase transitions, Phys. Rev. E **64**, 020901(R) (2001).

[59] N. Delorme and A. Fery, Direct method to study membrane rigidity of small vesicles based on atomic force microscope force spectroscopy, Phys. Rev. E **74**, 030901(R) (2006).

[60] A. Schlaich, J. Kappler, and R. R. Netz, Hydration friction in nanoconfinement: From bulk via interfacial to dry friction, Nano Lett. **17**, 5969 (2017).

[61] See Supplemental Material at http://link.aps.org/supplemental/10.1103/PhysRevFluids.7.114801 for animated versions of displacement plots, pressure profiles, and velocity fields.

[62] J. L. Harden, H. Pleiner, and P. A. Pincus, Hydrodynamic surface modes on concentrated polymer solutions and gels, J. Chem. Phys. **94**, 5208 (1991).

[63] T. Hiraiwa and R. R. Netz, Systematic bottom-up theory for the viscoelastic response of worm-like chain networks, EPL (Europhys. Lett.) **123**, 58002 (2018).

[64] J. M. Carcione, *Wave Fields in Real Media: Wave Propagation in Anisotropic, Anelastic, Porous and Electromagnetic Media*, 2nd ed., Handbook of Geophysical Exploration: Seismic Exploration (Elsevier Science, Amsterdam, 2007).

[65] I. A. Viktorov, *Rayleigh and Lamb Waves: Physical Theory and Applications*, Ultrasonic Technology (Plenum Press, New York, 1967).

[66] R. D. Borcherdt, *Viscoelastic Waves in Layered Media* (Cambridge University Press, Cambridge, 2009).

[67] U. Seifert and S. A. Langer, Viscous modes of fluid bilayer membranes, Europhys. Lett. (EPL) **23**, 71 (1993).

[68] F. Behroozi, J. Smith, and W. Even, Stokes' dream: Measurement of fluid viscosity from the attenuation of capillary waves, Am. J. Phys. **78**, 1165 (2010).

[69] G. Espinosa, I. López-Montero, F. Monroy, and D. Langevin, Shear rheology of lipid monolayers and insights on membrane fluidity, Proc. Natl. Acad. Sci. USA **108**, 6008 (2011).

[70] A. D. Dinsmore, M. F. Hsu, M. G. Nikolaides, M. Marquez, A. R. Bausch, and D. A. Weitz, Colloidosomes: Selectively permeable capsules composed of colloidal particles, Science **298**, 1006 (2002).

[71] D. Needham, Cohesion and permeability of lipid bilayer vesicles, in *Permeability and Stability of Lipid Bilayers*, edited by E. A. Disalvo and S. A. Simon (CRC Press, 1995), pp. 49–76.

[72] T. E. Thompson, M. B. Sankaram, and C. Huang, Organization and dynamics of the lipid components of biological membranes, in *Comprehensive Physiology* edited by R. Terjung (John Wiley & Sons, Ltd, 2011), pp. 23–57.

[73] M. Saeedimasine, A. Montanino, S. Kleiven, and A. Villa, Role of lipid composition on the structural and mechanical features of axonal membranes: A molecular simulation study, Sci. Rep. **9**, 8000 (2019).

[74] H. Meyer, Zur Theorie der Alkoholnarkose, Archiv Exp. Pathol. Pharmakol. **42**, 109 (1899).

[75] C. E. Overton, *Studien über die Narkose zugleich ein Beitrag zur allgemeinen Pharmakologie* (G. Fischer, Jena, 1901).

[76] R. S. Cantor, The lateral pressure profile in membranes: A physical mechanism of general anesthesia, Biochemistry **36**, 2339 (1997).

[77] R. A. Lerner, A hypothesis about the endogenous analogue of general anesthesia, Proc. Natl. Acad. Sci. USA **94**, 13375 (1997).

[78] B. W. Urban, M. Bleckwenn, and M. Barann, Interactions of anesthetics with their targets: Non-specific, specific or both? Pharmacol. Therapeut. **111**, 729 (2006).

[79] M. A. Pavel, E. N. Petersen, H. Wang, R. A. Lerner, and S. B. Hansen, Studies on the mechanism of general anesthesia, Proc. Natl. Acad. Sci. USA **117**, 13757 (2020).

[80] S. I. Rubinow and J. B. Keller, Wave propagation in a fluid-filled tube, J. Acoust. Soc. Am. **50**, 198 (1971).

[81] S. I. Rubinow and J. B. Keller, Wave propagation in a viscoelastic tube containing a viscous fluid, J. Fluid Mech. **88**, 181 (1978).

[82] J. R. Tyldesley, *An Introduction to Tensor Analysis for Engineers and Applied Scientists* (Longman, London, 1975).